

Estimating the fluid composition after dolomitization using mass balance equation: comparison of examples from Spain, Canada and France

Centrella, S.^a, Hoareau, G.^a, Beaudoin, N.E.^a, Motte, G.^a, Lanari, P.^b, Piccoli, F.^b, Callot, J.-P.^a, Gomez-Rivas, E.^c, and Martín-Martín, J.D.^c

^a Université de Pau et des Pays de l'Adour, E2S UPPA, LFCR, CNRS, TotalEnergies, Pau, France

^b Institut für Geologie, Universität Bern, Baltzerstrasse 3, CH-3012 Bern, Switzerland

^c Departament de Geoquímica, Petrologia i Prospecció Geològica, Universitat de Barcelona, Martí i Franquès s/n, 08028 Barcelona, Spain

This is a post-print version of the article:

Centrella, S., Hoareau, G., Beaudoin, N.E., Motte, G., Lanari, P., Piccoli, F., Callot, J.-P., Gomez-Rivas, E., and Martín-Martín, J.D. 2023. Estimating the fluid composition after dolomitization using mass balance equation: comparison of examples from Spain, Canada and France. *Global and Planetary Change*, 220, 104016.

DOI: <https://doi.org/10.1016/j.gloplacha.2022.104016>

For the final copy-edited version please visit:

<https://www.sciencedirect.com/science/article/pii/S0921818122002831>

Highlights

- We determined the partial fluid composition in equilibrium with dolomite after the reaction
- We determined the trace element exchange partition coefficient between dolomite and the fluid in equilibrium
- We determined the amount of fluid (seawater or basinal brine) required to replace a cubic meter of limestone

Keywords: Dolomitization; Fluid composition; Mass transfer; Diagenesis

Abstract

Dolomitization (i.e. replacement of CaCO_3 by $\text{CaMg}(\text{CO}_3)_2$) is a major mineralogical replacement process that affects limestones in numerous carbonate platforms, basins and fold-and-thrust belts worldwide. This phenomenon makes an important part of the carbon cycle, and large-scale dolomite geobodies that develop in nature are prime targets for greenhouse gas storage, or are related to ore deposit bearing rare metals, oil and gas reservoirs and geothermy. Yet, the conditions favoring dolomitization remain debated, specifically the major and trace element composition of the reactive aqueous fluid. In this contribution, we quantify the mass transfer between the original calcite and the newly formed dolomite in various natural cases of dolomitization, by coupling EPMA and LA-ICP-MS measurements, following a mass balance approach. This approach also allows to estimate the theoretical composition of an aqueous fluid whose element content would be provided by the reaction (i.e., in equilibrium with dolomite), as well as the partition coefficient for most elements involved in the reaction. This approach was tested using three existing datasets obtained from natural dolomite and original limestone in both Jurassic outcrops of the Layens anticline in the Pyrenees (France), and two from the Middle Devonian Pine Point Formation from the Presqu'île barrier (Canada). These are

complemented with new data acquired from Cretaceous limestones of the Benassal Formation in the Maestrat Basin (Spain). In these areas, dolomitization occurred at different T conditions (~ 50 to ~ 300 °C), from different fluid sources (seawater, basinal brines), and in different geodynamic settings. Yet, for all the studied examples, the dolomitization reactions result in similar solid volume variations (-14 to -10 vol%), the fluid in equilibrium with the dolomite have comparable trace element concentrations, and the partition coefficients calculated for all trace elements are consistent with each other. In addition to providing information with regards to the composition of the solid and fluid phases involved in the reaction, these results also suggest similar mechanisms of dolomitization in distinctly different geological contexts.

1. Introduction

Fluid-mediated mineral replacement, also defined as metasomatism, is a multiscale process not only altering the mineralogy, but also the composition and mechanical properties of rocks (Putnis, 2002, Putnis, 2009). In diagenetic to low-grade metamorphic conditions (< 300 °C), the consequences of such replacements are numerous, ranging from global element cycling (Whitaker et al., 2004; Ague and Nicolescu, 2014) to the accumulation of georesources, the modification of reservoir properties or fluid storage (Kirschner and Barnes, 2009; Thibeau et al., 2013). A well-known example of fluid-mediated mineral replacement under these conditions is dolomitization, where calcite (CaCO_3) is replaced by dolomite ($\text{Ca,Mg}(\text{CO}_3)_2$) (Warren, 2000; Machel, 2004). Analysis of natural dolomites using various approaches such as the study of their trace element or isotopic composition, or of fluid inclusions, have made it possible to define how an original limestone can become dolomitized to dolostone in specific geological environment (Davies and Smith, 2006; Al-Helal et al., 2012; Barale et al., 2016; Salardon et al., 2017; Koeshidayatullah et al., 2020; Motte et al., 2021). Two cases can be considered: the first occurs early after limestone deposition, at low temperature (e.g. Warren, 2000; Machel, 2004). It is favored by the involvement of Mg-rich waters such as evaporated seawater (e.g. Nader et al., 2012), by the mixing of seawater and continental water (e.g. Wilson et al., 1990; Gasparrini et al., 2006; Nader et al., 2012), or by bacterial activity (e.g. Slaughter and Hill, 1991). The second, occurring at greater depth during burial, involves the influx of hydrothermal Mg-rich water mainly through faults and fractures during tectonic deformation (Swennen et al., 2012; Martín-Martín et al., 2015; Mozafari et al., 2019). The latter presents an important economic interest due to the common formation of base metal deposits (Pb-Zn) along with dolomitization (Wallace et al., 1994; Diehl et al., 2010; Gomez-Rivas et al., 2014; Kelka et al., 2015; Martín-Martín et al., 2015; Kelka et al., 2017). Numerous experiments and thermodynamic and/or kinetic modelling have also focused on the conditions favorable to dolomitization (Bénézeth et al., 2018; Yang et al., 2022). They have shown, in accordance with field observations, that such replacement is increasingly favored with increasing temperature, and requires Mg-rich aqueous fluids to be efficient (Jonas et al., 2015; Jonas et al., 2017). However, several complications arise as to compare experimental results of solubility products and precipitation / dissolution kinetics with natural examples. These are due for example to the difference in composition between natural and experimental aqueous fluids driving dolomitization, changing the behavior of their interaction with Ca-Mg carbonates at the crystal scale (Möller and de Lucia, 2020). Such limitations do not allow to solve simple questions such as the precise amount of water needed, for a given composition, to replace a given volume of calcite by dolomite.

In this contribution, we propose a simple approach to quantify the mass transfer associated to dolomitization. It is based on the analysis of the composition of the initial calcite and newly formed dolomite in several natural dolomitization replacement fronts, while estimating the solid volume variation tied to the reaction. The application of mass transfer calculations, following the approach initially presented by Gresens (1967), allows the redistribution of the chemical elements analyzed between the solid phases during the reaction to be determined. This has led Centrella et al. (2020) to show that dolomitization results in a net mass loss of ~ 7 wt%, while Mg is incorporated in the solid structure of dolomite, and Ca as well as other trace elements are released out of it (i.e., removed from the system through the fluid phase) (Fig. 1). Applying

mass transfer calculations to three examples of natural dolomitization fronts makes it possible to identify and compare precisely the types and amounts of elements retrieved or released by the reaction. It also allows (i) to estimate the theoretical composition of an aqueous solution whose dissolved elements would only be supplied by the reaction, which helps (ii) to calculate the minimal volume of water of fixed Mg concentration necessary for a complete calcite-dolomite replacement, and (iii) to estimate partition coefficients between dolomite and water, which are still ill-defined for most trace elements.

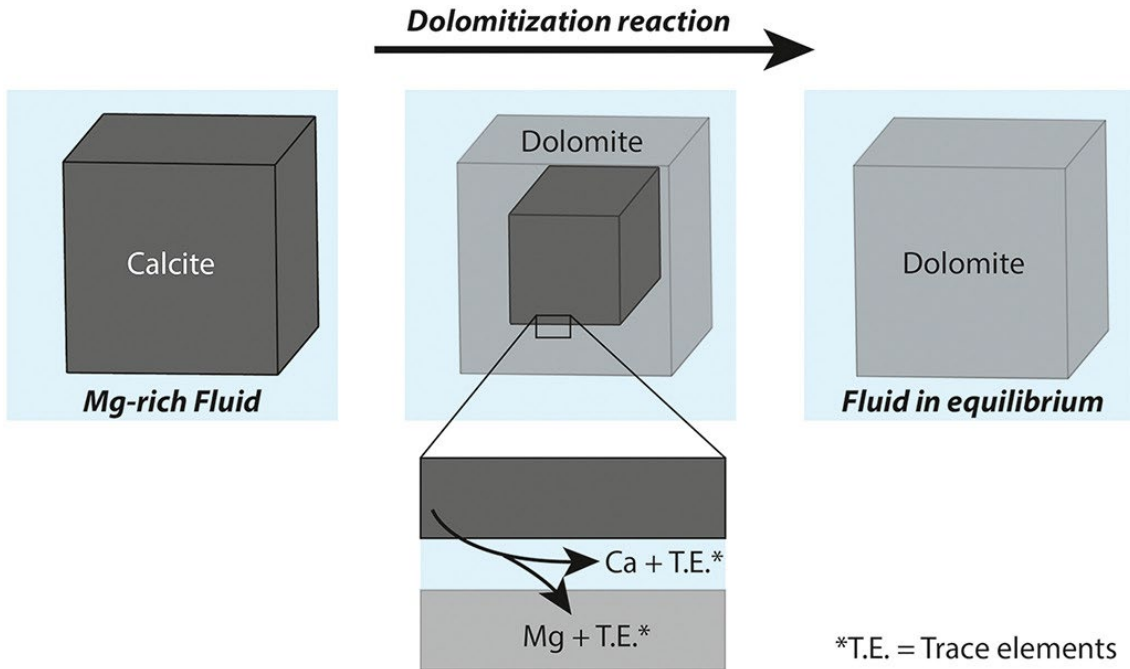


Fig. 1. Schematic sketch illustrating the entire replacement of calcite by dolomite.

To test this approach, aiming to improve our knowledge about the calcite-to-dolomite reaction and which can be applied anywhere where a reaction front is identified, we use published datasets of dolomitization from the Meillon Formation in the Layens anticline (French Pyrenees, Centrella et al. (2020)) and the Middle Devonian Pine Point Formation from the Presqu'île Barrier (Canada) (Qing and Mountjoy, 1994a, Qing and Mountjoy, 1994b, Qing and Mountjoy, 1994c), as well as new data acquired in Cretaceous limestones and dolostones of the Benassal Formation, in the Maestrat Basin (Spain). The three regions (from France, Spain, and Canada) describe dolomitization reactions occurring at different T conditions (~ 50 to ~ 300 °C), from different fluid sources (seawater, basinal brines), and in different geodynamic contexts.

2. Geological settings of the three study areas

2.1. The Layens anticline, Pyrenees, France

Dolomitization fronts are well preserved in limestones of the Meillon Formation (Motte, 2020), as part of the Layens anticline, an $E-W$ striking fold parallel to the Pyrenees and located in the Northern Pyrenean zone (Labaume and Teixell, 2020) (Fig. 2). These marine, bioclastic limestones developed in a ramp to rimmed shelf setting during Callovian to Oxfordian times (Motte, 2020), in a stable to slightly extensive tectonic context (Puigdefàbregas and Souquet, 1986). They overlie Upper Triassic evaporites and marls (Keuper Marls) and Early-Middle Jurassic interbedded marls and limestones (Aussurucq Limestones), and are covered by Upper Jurassic argillaceous limestones (Lons Limestones), followed by reef limestones (Lenoble, 1992). Based on paleofluid characterization, it has been proposed that dolomitization of the Meillon Formation relates to the flow of hydrothermal magmatic fluids between ~ 200

and ~ 300 °C (Motte et al., 2021), ascending along faults that became hypersaline in contact with the Triassic evaporites (Salardon et al., 2017). The dolomitization event was synchronous with rifting associated to crustal thinning (Salardon et al., 2017; Incerpi et al., 2020) that affected the area during the Albian-Cenomanian, and which resulted in a geothermal gradient of around ~80 °C/km (Vacherat et al., 2014). Anticline fold development started during the formation of salt diapirs at that time, and was amplified during subsequent shortening and continental collision at the origin of the Pyrenean orogen from the late Santonian (~80 Ma) culminating in the Middle tertiary (Mouthereau et al., 2014; Teixell et al., 2016; Izquierdo-Llavall et al., 2020; Labaume and Teixell, 2020).

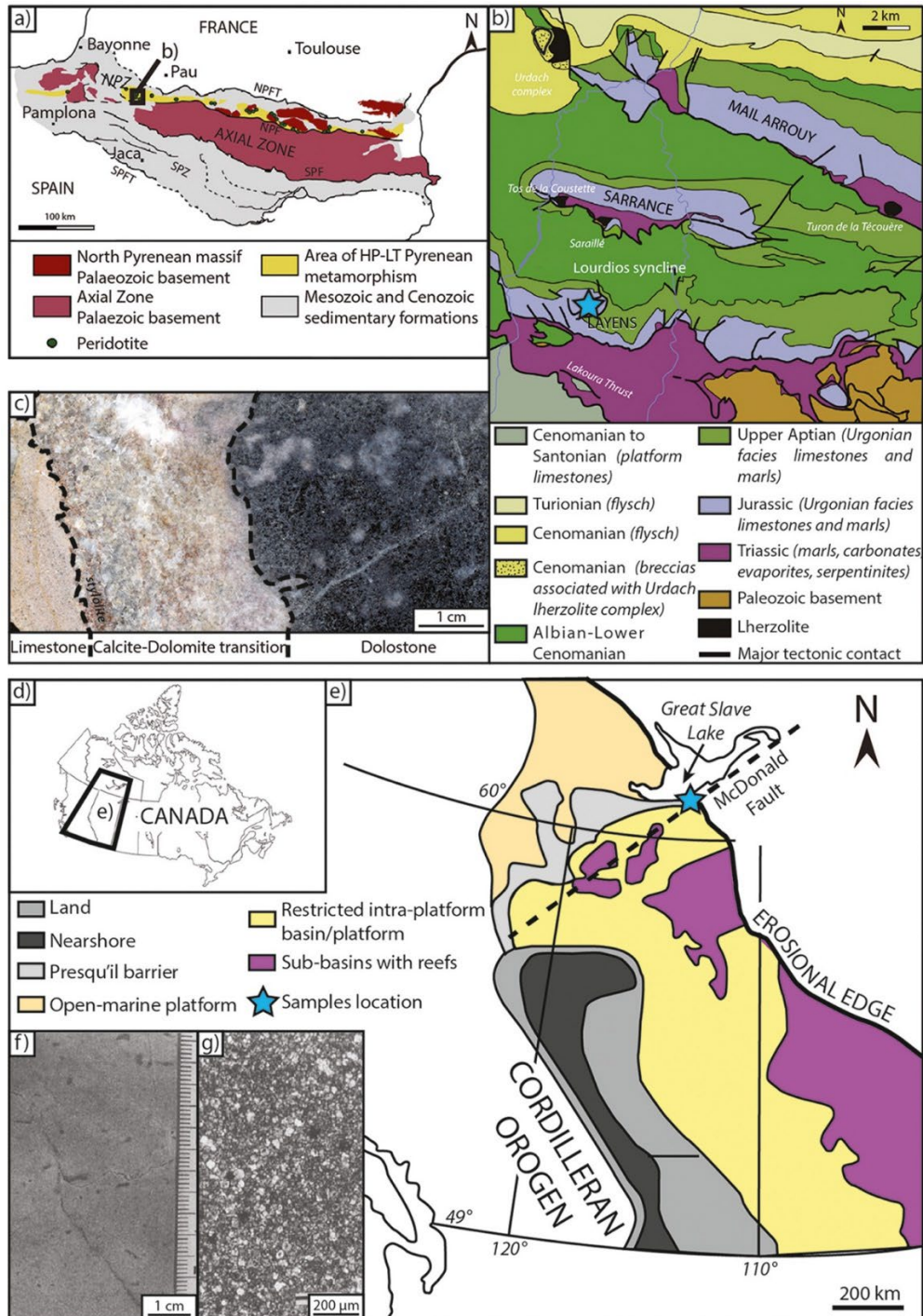


Fig. 2. Location of two published studies of the Layens region Centrella et al. (2020) (a, b) and Presqu'île Barrier region (modified from Qing (1998)). High resolution two-dimensional scan of a polished slab of limestone and dolostone from the Meillon Formation of the Layens region (c, modified from Centrella et al. (2020)) and from the Pine Point Formation of the Presqu'île Barrier (modified from Qing (1998)).

2.2. The Pine Point Formation from the Presqu'île barrier, Canada

The regional geology of the Presqu'île barrier (Fig. 2), a Middle Devonian carbonate reef complex located in the Western Canada Sedimentary Basin (WCSB), has been extensively described since the early work of Jackson and Beales (1967). Its development resulted in restricted seawater circulation in the southern part of the WCSB, where evaporites and carbonates were deposited, contrasting with the open marine carbonates and shales deposited north of the barrier (Qing and Mountjoy, 1994c; Qing, 1998). The barrier comprises the Pine Point and Sulphur Point Formations, that were deposited above the Keg River Formation, a regional shallow platform made of dolostones with abundant crinoid and brachiopods fragments. The Pine Point Formation was originally deposited as marine limestones, but the latter have been variably dolomitized at around 50 °C by seawater-derived fluids (Qing and Mountjoy, 1994c; Qing, 1998; Adams et al., 2000). No clear dolomitization front are described in these studies. Gradually to the south, the Pine Point Formation evolves into evaporitic, fine crystalline dolomite and anhydrite. Early after its development, the Presqu'île barrier was exposed, giving rise to the sub-watt Mountain unconformity (Meijer Drees, 1988). It was then invaded by evaporitic brines followed by meteoric water (Qing and Mountjoy, 1990). Therefore, diagenetic sequence of the barrier is as follow. A first event occurring in submarine environment presents features like syntaxial, microspar and fibrous cements, and fine crystalline dolomite (Qing and Mountjoy, 1990). A latter event in subaerial conditions formed minor and localized cements with minor dissolution and brecciation features (Qing and Mountjoy, 1994b). The last event at subsurface produced blocky sparry cements of calcite, compaction and stylolitization, crystalline and saddle dolomites, sulphide mineralization, calcite and a late stage of calcite, fluorite, and pyrobitumen formation (Qing and Mountjoy, 1994a).

2.3. The Benassal Formation, Maestrat basin, Spain

The Maestrat basin, located to the East of the Iberian peninsula, was formed as a consequence of a Late Jurassic – Early Cretaceous rifting cycle (Salas and Casas, 1993; Salas et al., 2001). In its southern part (Benicàssim area), where Paleozoic basement, Permian-Triassic rocks and the Jurassic-Cretaceous cover are well exposed (Roca and Guimerà, 1992), the basin is bounded by two sets of major faults that controlled the sedimentation and later on, fluid circulation and associated dolomitization along the Benicàssim (NNE-SSW trending and ESE dipping) and the Campello (EW trending, S dipping) faults (Roca and Guimerà, 1992; Gomez-Rivas et al., 2012; Martín-Martín et al., 2013). These pre-rift structures were reactivated as normal faults during the Mesozoic rifting, as strike-slip and reverse oblique-slip faults during the Tertiary inversion that formed the Iberian Chain (Guimerà et al., 2004), and again as normal faults during the Neogene extension that formed the Valencia Trough and the western Mediterranean basin (Roca and Guimerà, 1992; Gomez-Rivas et al., 2012). In the same area, the Benassal Formation was deposited between the Late Aptian and Early Albian (Moreno-Bedmar et al., 2010; Martín-Martín et al., 2013; Garcia et al., 2014). It mostly consists of shallow-marine limestones with rudist bivalves, corals, algae-rich facies and orbitolinid foraminifera (Tomàs et al., 2007; Bover-Arnal et al., 2009; Martín-Martín et al., 2013). The succession is characterized by three transgressive-regressive sequences, and is overlain by the Escucha Formation (Rodríguez-López et al., 2007). In the Benassal Formation, the largest exposed dolostones are located in the hanging walls of the Campello and Benicàssim faults (Fig. 3). They mostly replace the original peloidal packstones to grainstones, and the bioclastic wackestones to packstones (Martín-Martín et al., 2012; Martín-Martín et al., 2013). The original depositional facies exerted a strong control on the lateral fluid flow along the most permeable layers, favoring a stratabound dolostone geometry away from the faults (Martín-Martín et al., 2013; Corbella et al., 2014). Replacement occurred with supposedly hydrothermal fluids exceeding 80 °C, and allowing the formation of MVT (Mississippian Valley Type) sulphide mineralization (Martín-Martín et al., 2013; Martín-Martín et al., 2015). No clear dolomitization front are described in these studies.

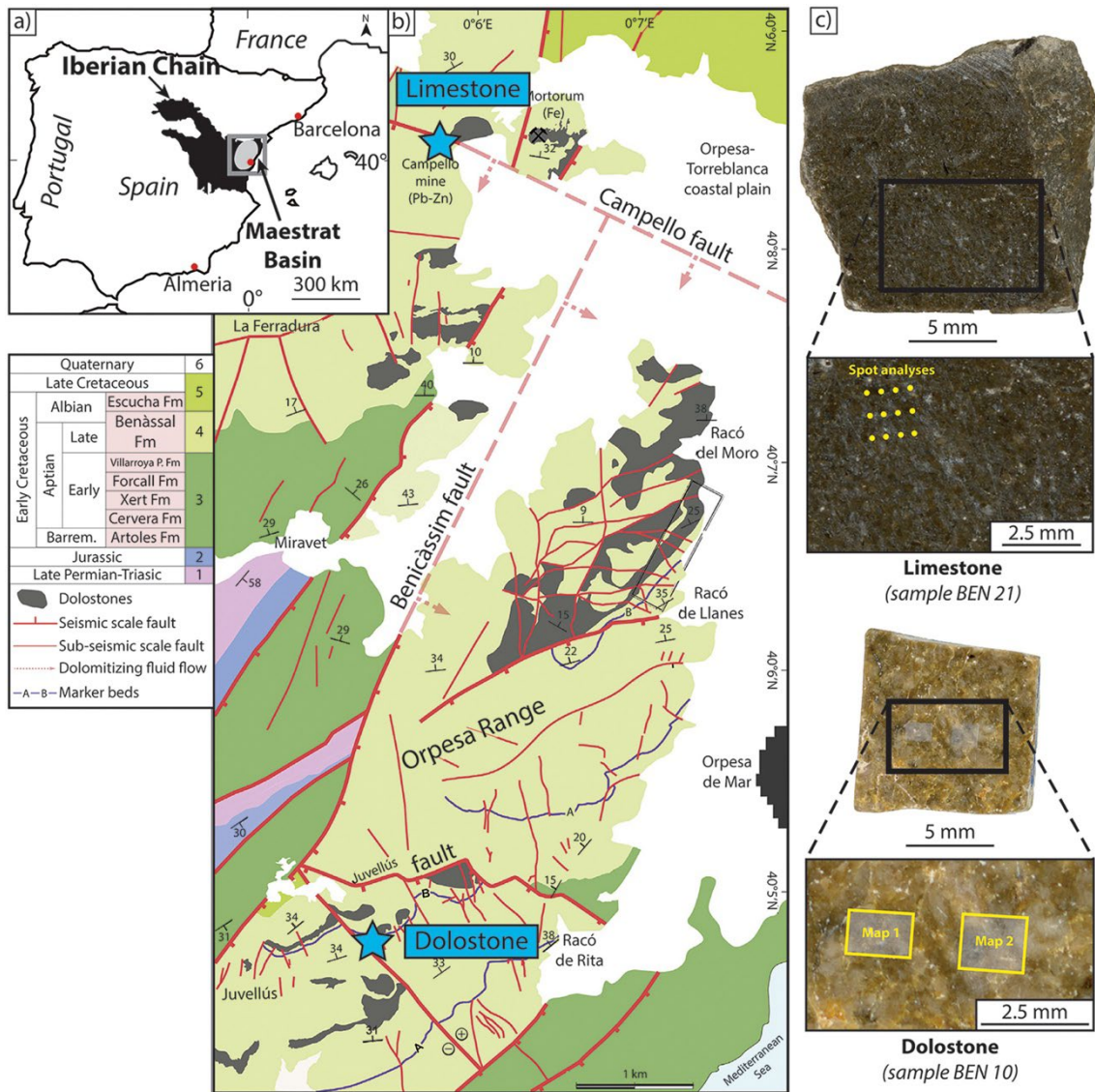


Fig. 3. Location of the new study area of the Benassal Formation, Spain (modified from Martín-Martín et al. (2015)). High resolution two-dimensional scan of a polished slab of limestone and dolostone (c).

3. Material and methods

3.1. Sample collection

A set of 21 samples were collected in limestones and dolostones of the Benassal Formation of the Maestrat basin. From these, one limestone and one dolostone sample coming from the vicinity of the Campello mine were chosen to be analyzed for trace elements (Fig. 3c). One of the difficulties about the Benassal Formation is the actual preservation of dolostone because a late dedolomitization event occurs and alter it. We used the better sample found without any alteration. A detailed petrographic study of the limestone, which was formed almost entirely in shallow-water marine environment, is provided in Tomàs et al. (2007). The dolostones were studied in detail by Martín-Martín et al. (2010) and Martín-Martín et al. (2013). For the Layens anticline, trace element data are taken from Centrella et al. (2020). For the Presqu'île Barrier, they come from Qing and Mountjoy (1994c) with compositions of two original limestone (PP-2822-239 and PP-2822-246) and one dolostone (NWT-F51-4964).

3.2. Trace element concentration

For the Benassal Formation samples, two polished blocks of around 8x8x4 mm of limestone and dolostone were prepared to measure the trace element content (Fig. 3c). Chemical compositions were measured with a femtosecond laser ablation system (Lambda3; Nexeya, Bordeaux, France) coupled to a high resolution ICP-MS Element XR fitted with the Jet Interface (fsLA/HR-ICP-MS) (Thermo Fisher Scientific, Waltham, MA, USA). For the limestones, analyses were based on in situ laser ablation spots (17 μm size), whereas for dolostone they were based on trace element mapping using successive line rasters (Centrella et al., 2020). Measurements were performed under dry plasma conditions. The additional Ar carrier gas flow rate, torch position and power were adjusted so that the U/Th ratio was close to 1 \pm 0.05 when ablating the glass SRM NIST612. The reference materials NIST612 and NIST610 were respectively used as primary and secondary calibration standard. ^{43}Ca was used as internal standard for calcite quantification, and ^{25}Mg for dolomite (Jochum et al., 2011). Detector cross-calibration and mass bias calibration were checked daily using the appropriate sequence of the Element Software. ^{25}Mg , ^{43}Ca , ^{57}Fe , ^{55}Mn , ^{51}V , ^{66}Zn , ^{85}Rb , ^{88}Sr , ^{89}Y , ^{139}La , ^{140}Ce , ^{141}Pr , ^{146}Nd , ^{150}Sm , ^{153}Eu , ^{158}Gd , ^{159}Tb , ^{163}Dy , ^{165}Ho , ^{166}Er , ^{169}Tm , ^{172}Yb , ^{175}Lu , ^{208}Pb and ^{238}U were selected in low resolution mode ($R = 300$) with a dwell time of 30 ms. Images were built from the signal resulting from the sample ablation according to a series of vertically distributed horizontal lines, with a scan speed of 1 $\text{mm}\cdot\text{s}^{-1}$ and a sample translation set to 17 $\mu\text{m}\cdot\text{s}^{-1}$ giving pixels of 17 \times 17 μm . Helium stream was fixed to 500 $\text{mL}\cdot\text{min}^{-1}$. For the Meillon and the Benassal Formation, phase segmentation was performed by the random forest algorithm present in XmapTools 4 using trace elements maps. It is an ensemble learning method for classification constructing a multitude of decision trees during training. The output of the random forest is the class selected by most tree, in our case, minerals. For the Meillon Formation, local bulk compositions of calcite and dolomite were extracted from trace element maps after phase segmentation (Centrella et al., 2020), as the local bulk composition of dolomite for the Benassal Formation. For the Pine Point Formation, samples come from petroleum drill wells. The rock sample were dissolved and measured in an inductively coupled plasma mass spectrometer (ICP-MS) using the method of standard additions to correct for matrix effects (Qing and Mountjoy, 1994c). Unfortunately, this method doesn't allow us to properly measure the calcite and the dolomite chemical composition because other minerals can be present in the sample such as clays.

3.3. Mass balance equation

Mass balance calculations as defined by Gresens (1967) or Grant (1986) can be used to quantify element mobility during a fluid-mediated mineral/rock replacement, provided that the density variation and the volume change between the original mineral or rock and the newly formed mineral assemblage are known (Ague, 1991; Centrella et al., 2015, Centrella et al., 2016; Centrella et al., 2018; Centrella, 2019). Both calculations assume that only one fluid is responsible for the reaction, and that its chemical composition remains constant during the reaction. Since the study is focused on dolomitization, the same mass balance equation is used for the three case studies where an original limestone composed by calcite is replaced by a dolostone composed by dolomite, using the Gresens equation, which is valid in an open system (Eq. 1):

$$f_v \times \left(\frac{d_{\text{Dolomite}}}{d_{\text{Calcite}}} \right) \times C_{\text{Dolomite}}^{\text{Element}} - C_{\text{Calcite}}^{\text{Element}} = x_{\text{Element}} \quad (1)$$

With f_v the volume factor corresponding to the variation of the solid volume during the reaction, d the phase density ($\text{g}\cdot\text{cm}^{-3}$) C the element concentration measured in a given mineral (oxide weight %) and x the mass change (in grams). Positive values correspond to a gain of mass (i.e. elements were brought by the fluid phase) and negative values to a loss of mass (i.e. elements were released to the fluid phase). For a value of $f_v = 1$, no solid volume change is involved between the reactants and the products. Values of $f_v > 1$ and $f_v < 1$ correspond to volume increase or decrease of the solid phase, respectively. The concentration of Ca, Mg, Fe and Mn in dolomite and calcite were used to calculate the density of the mineral phases, by assuming that

each element concentration directly relates to the proportion of pure mineralogical end-member in a mineral that is a linear solid solution between these end-members. Although there is a difference between assuming that linear mixing on molar volumes is not the same as density, this approximation yields to a negligible difference with thermodynamic computed density (Centrella et al., 2018). For the calcite system, the pure end-members consists of calcite (Ca, density 2.74 g.cm⁻³), magnesite (Mg, density 2.98 g.cm⁻³), siderite (Fe, density 3.87 g.cm⁻³) and rhodochrosite (Mn, density 3.70 g.cm⁻³) (Graf, 1961). For dolomite the end-members consist of dolomite (Mg, density 2.84 g.cm⁻³), ankerite (Fe, density 3.15 g.cm⁻³) and kutnohorite (Mn, density 3.08 g.cm⁻³) (Steinfink and Sans, 1959; Graf, 1961; Reeder and Dollase, 1989). Two ways can be used to determine f_v : the first is by considering either one or several immobile elements during the reaction, and the second is by minimizing the total mass transfer associated to the reaction (Hermann et al., 2013). The latter approach was used in the present study, since it was successfully applied to dolomitization reactions by Centrella et al. (2020). Minimization of the mass transfer consists in solving Eq. 1 for each element of which its concentration was measured, and for considering a range of f_v values. This allows to define the Solid volume variation (%), plotted as the sum of the mass change x for all elements against the range of f_v values, and which corresponds to the following equation (Eq. 2):

$$\text{Solid volume variation (\%)} = (-1 + f_v) \times 100 \quad (2)$$

The optimal volume factor $f_v \text{ opt}$ corresponds to the minimum of the solid volume variation (Centrella et al., 2020). The mass transfer between the original limestone and the newly formed dolostone is plotted in an isocon diagram (Grant, 1986, Grant, 2005) using the percentage of mass change obtained with the Gresens equation and the optimal volume factor. If considering an error of $\pm 5\%$ on the estimate of the optimal volume factor, the error on the estimate of the element mass change represents $< 2\%$ for trace elements and about 9% for major elements (Ca, Mg, Fe, Mn). These values are negligible with respect to the ranges of mass change variations observed.

3.4. Amount of fluid and its composition

Various models have been developed to calculate the amount of fluid required to perform a mineral replacement (Baumgartner and Ferry, 1991; Staude et al., 2009; Weisheit et al., 2013; Gomez-Rivas et al., 2014). The mass of Mg required to achieve dolomitization is by far the largest cation so we present such calculations using Mg as a reference (Gomez-Rivas et al., 2014). Using the result of the mass balance equation (Eq. 1), one can estimate the amount of fluid required to replace 100 g of original calcite by fixing the Mg concentrations of the input fluid. Since seawater and basinal brines are commonly involved in natural dolomitization reactions (Nader et al., 2012; Swennen et al., 2012; Martín-Martín et al., 2015; Mozafari et al., 2019), calculations were made with two Mg concentrations, the first being similar to that of seawater (1.29 g/L or 0.0531 mol/kg; Stumm and Morgan (1981)), and the second to that of a basinal brine (3.05 g/L or 0.1255 mol/kg; Kharaka and Thordsen (1992)). Here, we fixed a Mg concentration for seawater and brine to illustrate the method proposed even though their composition varies over time (Gabellone and Whitaker, 2016). Assuming that this Mg content of the dolomitizing fluid is constant during the reaction (i.e. an infinite supply of reactant), the theoretical composition of the aqueous fluid whose dissolved content would only result from the reaction (apart from Mg) can be calculated for all measured elements other than Mg, using Eq. 3:

$$\frac{X_n}{Q} \times 1000 = C_n^{\text{solution}} \quad (3)$$

With X_n the mass of element provided by the reaction (negative values in gram), Q the amount of fluid required to replace 100 g of calcite (in liter), and C_n^{solution} the concentration of an element n in the fluid (mg/L). This composition can be compared to that of an initial water with Mg as dissolved species, which would be put in contact with dolomite until equilibrium is

reached. Applying the calculation to the 3 natural cases studied here, it also corresponds to the minimum concentration of each element present in the fluid phase after dolomitization.

3.5. Exchange partition coefficient

The relationship between the distribution of two elements i and j in the solid and the fluid phase at equilibrium is usually quantified using an exchange partition (or distribution) coefficient K_D^{i-j} , defined as Banner and Hanson (1990):

$$K_D^{i-j} = \left(C_s^i / C_s^j \right) / \left(C_f^i / C_f^j \right) \quad (4)$$

where C_s^i and C_s^j are the mass fractions of the elements i and j in the solid, and C_f^i and C_f^j the mass fractions of the elements i and j in the fluid. This equation conveniently applies to element substitution in minerals, where i would be the trace element that substitutes to a major element j (Banner and Hanson, 1990). Regarding dolomite, both crystallographic sites containing Ca and Mg can be involved in cation substitution, where cations smaller than Mg should use the Mg site, and the larger ones should preferentially substitute for Ca (Kretz, 1982). By studying the substitution of Ni, Cu, Co, Zn, Hg, Pb, Fe, Mn, Ba and Sr in dolomite, Kretz (1982) proposed that Ni, Cu, Co, Fe and Mn essentially use the Mg site, whereas other elements substitute mostly for Ca. For the sake of simplicity, it is assumed here that all the analyzed trace elements substitute with Ca. The element exchange partition coefficients can thus be expressed as:

$$K_D^{\text{Element}-\text{Ca}} = \left(C_{\text{Solid}}^{\text{Element}} / C_{\text{Solid}}^{\text{Ca}} \right) / \left(C_{\text{Fluid}}^{\text{Element}} / C_{\text{Fluid}}^{\text{Ca}} \right) \quad (5)$$

With $C_{\text{Solid}}^{\text{Element}}$ and $C_{\text{Fluid}}^{\text{Element}}$ the concentration or mass fraction of an element in the solid and in the fluid phase, and $C_{\text{Solid}}^{\text{Ca}}$ and $C_{\text{Fluid}}^{\text{Ca}}$ the concentration or mass fraction of Ca in the solid and fluid phase. Following Eq. 5, element concentrations measured in dolomite and theoretical element concentrations calculated for the fluid phase after the reaction (i.e., at equilibrium with dolomite) can be used to calculate minimum values of exchange partition coefficients for all measured elements that are released by the reaction.

4. Results

4.1. Petrography

The hand specimen of the Meillon Formation (Layens anticline) displays a dolomitization front characterized by three areas with distinct crystal sizes or mineralogies (Centrella et al., 2020; Fig. 2a-c): (i) a first area with small calcite crystals around 100 μm in size, with low porosity (< 1 vol%), and oxides located along grain boundaries, (ii) a second area made of dolomite crystals (< 600 μm in size) with a constant and homogeneous porosity around 2 vol%, and (iii) a third area located between the previous ones, made of coarse calcite crystals ranging from 200 μm to 1.5 mm in size, and with a porosity lower than 0.5 vol%. Closer to the dolomite area, calcite grain size decreases and porosity increases (< 1 vol%). Trace element analyses (fsLa-ICP-MS) were performed on thin sections made across the entire specimen, comprising the three areas (Centrella et al., 2020).

The limestones of the Pine Point Formation in the Presqu'île Barrier are characterized by a brown color and variable amount of crinoids, stromatoporoids and shell fragments (Qing and Mountjoy, 1994c). All fossils are embedded in a grainstone, cemented mainly by microspar and fibrous cements. The dolomite crystals range from 5 to 25 μm in size, are subhedral to euhedral and present a planar extinction (Fig. 2f and g). Dolomite samples have low porosity and permeability. The sedimentary structures and fossils are well preserved (Qing and Mountjoy, 1994c; Qing, 1998).

The limestone sample from the Benassal Formation in Spain. The studied sample corresponds to a dark grey bioclastic grainstone (Fig. 3c). For the dolostone sample, dolomite is present as

planar to non-planar crystals with a cloudy appearance (Fig. 3c). Grain size varies between 50 and 600 μm . Porosity is submillimetric and intercrystalline. For more details, see the more complete description in Martín-Martín et al. (2013).

4.2. Trace elements

For the sample from the Meillon Formation (Layens anticline), the trace element compositions obtained from fsLA-ICP-MS maps are presented in Table 1. REEs contents are rather similar between the calcite and the dolomite, but slightly less concentrated in the dolomite. Dolomite stoichiometry is considered as pure dolomite end-member with a Ca and Mg atomic per formulae unit (apfu) of 1.00 and 0.99 respectively (Centrella et al., 2020). Similar observations can be made for the REEs of the Pine Point Formation (Presqu'île Barrier) obtained by ICP-MS (Table 2) and for the dolomite stoichiometry with a Ca and Mg apfu of 1.01 and 0.98 respectively (Qing and Mountjoy, 1994c; Qing and Mountjoy, 1994b). For the new dataset of the Benassal Formation (Maestrat basin), the systematics in trace elements between the original limestone and the newly formed dolostone are similar except for Sr and Zn (Table 3).

Representative LA-ICP-MS phase and concentration maps of the analyzed dolostone sample are presented in Fig. 4. A slight chemical zonation is present for V but these variations are less important considering the mass balance calculation. The REE pattern of the original limestone presents a slight enrichment in heavy REEs compared to light REEs ($\text{La/Lu} = 0.81$, Fig. 5). The dolostone has a similar pattern, but with lower concentration for every REE. In general, dolostone REE pattern is positive with a general increase in concentration from LREE (light REE) to HREE (heavy REE). Both samples possess a positive anomaly in Sm and a negative anomaly in Tb, but the dolostone presents a positive anomaly in La and a negative anomaly in Ce. As described by Martín-Martín et al. (2015), dolomite contains some Fe giving dolomite stoichiometry of Fe (~ 0.04 apfu), Mg (~ 0.93 apfu) and Ca (~ 1.03 apfu).

Table 1. Average major and trace element composition of calcite and dolomite for the Layens, and calculated element mass changes (X_n), minimum element concentrations in the fluid in equilibrium with dolomite and K_D . Mass balance calculations suppose a variation of the solid volume of about -11.3% (Centrella et al., 2020). Fluid compositions were obtained assuming a fluid with a Mg content of 3.05 g/L similar to a basinal brine (Kharaka and Thordsen, 1992), and with a seawater Mg content of 1.29 g/L (Stumm and Morgan, 1981). CO_2 concentration was obtained by difference between 100 and the sum of all element oxide weight percent, then converted in element weight percent.

Table 1. Average major and trace element composition of calcite and dolomite for the Layens, and calculated element mass changes (X_n), minimum element concentrations in the fluid in equilibrium with dolomite and K_D . Mass balance calculations suppose a variation of the solid volume of about -11.3% (Centrella et al., 2020). Fluid compositions were obtained assuming a fluid with a Mg content of 3.05 g/L similar to a basinal brine (Kharaka and Thordsen, 1992), and with a seawater Mg content of 1.29 g/L (Stumm and Morgan, 1981). CO_2 concentration was obtained by difference between 100 and the sum of all element oxide weight percent, then converted in element weight percent.

	Calcite (wt%)	Dolomite (wt%)	X_n (mass change in gram)	X_n (mass change in %)	Fluid composition in equilibrium with 3.78L of brine source (mg/L)	Fluid composition in equilibrium with 8.94L seawater source (mg/L)	K_D^{Elem-} Ca
Al	0.01	0.00	-0.004	-55	1.138	0.481	0.79
Fe	0.01	0.02	0.007	86	-	-	-
Mn	0.03	0.03	-0.003	-10	0.824	0.349	9.00
Mg	0.09	12.51	11.532	12,375	-	-	-
Ca	37.99	20.74	-18.710	-49	4948	2093	-
Na	4.40E-03	7.98E-03	0.003	69	-	-	-
K	4.38E-03	9.93E-04	-0.003	-79	0.915	0.387	0.79
C	12.72	13.69	0.001	0	-	-	-
Li	5.30E-05	9.51E-05	3.54E-05	67	-	-	-
B	3.88E-05	7.00E-05	2.63E-05	68	-	-	-
Sc	1.32E-05	2.21E-05	7.39E-06	56	-	-	-
51V	8.15E-05	2.78E-04	1.77E-04	217	-	-	-
Cr	1.59E-04	3.18E-04	1.36E-04	86	-	-	-
Ni	1.27E-03	1.28E-03	-7.70E-05	-6	2.04E-02	8.62E-03	15.04
As	1.67E-04	3.13E-05	-1.38E-04	-83	3.66E-02	1.55E-02	0.20
Ba	9.23E-05	4.60E-05	-4.95E-05	-54	1.31E-02	5.54E-03	0.84
Zn	1.04E-02	1.56E-02	4.04E-03	39	-	-	-

Rb	1.94E-05	4.49E-06	-1.52E-05	-78	4.02E-03	1.70E-03	0.27
Sr	4.28E-02	1.31E-02	-3.07E-02	-72	8.110	3.430	0.38
Y	7.66E-04	4.78E-04	-3.21E-04	-42	8.49E-02	3.59E-02	1.34
La	4.85E-04	2.20E-04	-2.81E-04	-58	7.42E-02	3.14E-02	0.71
Ce	2.82E-04	1.09E-04	-1.81E-04	-64	4.78E-02	2.02E-02	0.54
Pr	5.53E-05	2.70E-05	-3.02E-05	-55	7.97E-03	3.37E-03	0.81
Nd	2.26E-04	1.14E-04	-1.20E-04	-53	3.18E-02	1.34E-02	0.86
Sm	4.24E-05	2.32E-05	-2.09E-05	-49	5.52E-03	2.34E-03	1.00
Eu	2.33E-05	5.63E-06	-1.80E-05	-78	4.77E-03	2.02E-03	0.28
Gd	5.81E-05	3.12E-05	-2.91E-05	-50	7.71E-03	3.26E-03	0.97
Tb	7.80E-06	4.71E-06	-3.43E-06	-44	9.06E-04	3.83E-04	1.24
Dy	5.19E-05	3.50E-05	-1.94E-05	-37	5.13E-03	2.17E-03	1.63
Ho	1.19E-05	8.53E-06	-3.93E-06	-33	1.04E-03	4.40E-04	1.96
Er	3.35E-05	2.71E-05	-8.28E-06	-25	2.19E-03	9.26E-04	2.98
Tm	3.71E-06	3.25E-06	-6.89E-07	-19	1.82E-04	7.70E-05	4.26
Yb	2.13E-05	2.23E-05	-6.25E-07	-3	1.65E-04	6.99E-05	32.17
Lu	2.98E-06	3.14E-06	-6.00E-08	-2	1.59E-05	6.71E-06	47.22
Pb	1.28E-04	4.65E-05	-8.45E-05	-66	2.24E-02	9.46E-03	0.50
Th	5.98E-06	8.16E-06	1.60E-06	27	-	-	-
U	2.65E-05	1.17E-04	8.27E-05	312	-	-	-

Table 2. Average major and trace element composition of calcite and dolomite for the Presqu'ile Barrier, and calculated element mass changes (X_n), minimum element concentrations in the fluid in equilibrium with dolomite and K_D . Mass balance calculations suppose a variation of the solid volume of about -10.5% . Fluid compositions were obtained assuming a fluid with a Mg content of 3.05 g/L similar to a basinal brine (Kharaka and Thordsen, 1992), and with a seawater Mg content of 1.29 g/L (Stumm and Morgan, 1981). CO_2 concentration was obtained by difference between 100 and the sum of all element oxide weight percent, then converted in element weight percent.

	Calcite	Dolomite	X_n (mass				
	Sample	Sample	change in	X_n	Fluid	Fluid	$K_D^{\text{Elem-}}$
	PP-2822-239	NWT-F51-	gram)	(mass	composition in	composition in	Ca
	(wt%)	4964	change	change	equilibrium	equilibrium	
		(wt%)	in %)	in %)	with 3.90L of	with 9.22L	
					brine source	seawater	
					(mg/L)	source (mg/L)	
Fe	0.30	0.14	-0.167	-56	43	18	0.71
Mn	0.01	0.01	3.88E-04	4	-	-	-
Mg	0.10	12.69	11.898	11,898	-	-	-
Ca	38.59	21.54	-18.388	-48	4714	1994	-
C	12.44	13.26	0.002	0	-	-	-
Sr	1.43E-02	5.70E-03	-9.00E-03	-63	2.31	0.98	0.54
La	1.98E-04	1.79E-04	-3.08E-05	-16	7.89E-03	3.34E-03	4.95
Ce	4.91E-04	1.91E-04	-3.12E-04	-64	8.00E-02	3.38E-02	0.52
Pr	6.35E-05	3.34E-05	-3.22E-05	-51	8.25E-03	3.49E-03	0.89
Nd	2.34E-04	1.36E-04	-1.07E-04	-46	2.74E-02	1.16E-02	1.09
Sm	4.63E-05	2.80E-05	-2.00E-05	-43	5.14E-03	2.17E-03	1.19
Eu	1.08E-05	6.30E-06	-4.89E-06	-45	1.25E-03	5.30E-04	1.10
Gd	4.38E-05	3.90E-05	-7.22E-06	-16	1.85E-03	7.83E-04	4.61
Tb	7.60E-06	5.00E-06	-2.91E-06	-38	7.46E-04	3.16E-04	1.47
Dy	4.18E-05	3.45E-05	-9.44E-06	-23	2.42E-03	1.02E-03	3.12
Ho	8.20E-06	7.00E-06	-1.63E-06	-20	4.19E-04	1.77E-04	3.66
Er	2.11E-05	2.09E-05	-1.50E-06	-7	3.84E-04	1.62E-04	11.92
Tm	2.90E-06	1.90E-06	-1.12E-06	-39	2.87E-04	1.21E-04	1.45
Yb	2.13E-05	1.68E-05	-5.54E-06	-26	1.42E-03	6.01E-04	2.59
Lu	2.70E-06	1.30E-06	-1.48E-06	-55	3.80E-04	1.61E-04	0.75

Calcite Sample PP-2822-246 (wt%)	X_n (mass change in gram)	X_n (mass change in %)	Fluid composition in equilibrium with 3.90L of brine source (mg/L)	Fluid composition in equilibrium with 9.22L seawater source (mg/L)	$K_D^{Elem-Ca}$
Fe 0.10	3.25E-02	33	-	-	-
Mn 0.01	3.00E-03	38	-	-	-
Mg 0.10	11.90	11,898	-	-	-
Ca 38.59	-18.39	-48	4714	1994	
C 12.51	-6.92E-02	-1	17.74	7.50	-
Sr 1.43E-02	-9.00E-03	-63	2.31	0.98	0.54
La 3.73E-04	-2.06E-04	-55	5.27E-02	2.23E-02	0.74
Ce 5.61E-04	-3.83E-04	-68	9.81E-02	4.15E-02	0.43
Pr 8.26E-05	-5.13E-05	-62	1.31E-02	5.56E-03	0.56
Nd 3.41E-04	-2.14E-04	-63	5.48E-02	2.32E-02	0.54
Sm 7.10E-05	-4.47E-05	-63	1.15E-02	4.85E-03	0.53
Eu 1.64E-05	-1.05E-05	-64	2.69E-03	1.14E-03	0.51
Gd 7.17E-05	-3.51E-05	-49	9.00E-03	3.81E-03	0.95
Tb 1.03E-05	-5.61E-06	-54	1.44E-03	6.08E-04	0.76
Dy 6.03E-05	-2.79E-05	-46	7.16E-03	3.03E-03	1.05
Ho 1.25E-05	-5.93E-06	-47	1.52E-03	6.43E-04	1.01
Er 3.07E-05	-1.11E-05	-36	2.84E-03	1.20E-03	1.61
Tm 4.40E-06	-2.62E-06	-59	6.71E-04	2.84E-04	0.62
Yb 2.17E-05	-5.94E-06	-27	1.52E-03	6.44E-04	2.41
Lu 3.00E-06	-1.78E-06	-59	4.56E-04	1.93E-04	0.62

Table 3. Average major and trace element composition of calcite and dolomite for the Benassal Formation, and calculated element mass changes (X_n), minimum element concentrations in the fluid in equilibrium with dolomite and K_D . Mass balance calculations suppose a variation of the solid volume of about -14.4%. Fluid compositions were obtained assuming a fluid with a Mg content of 3.05 g/L similar to a basinal brine (Kharaka and Thordsen, 1992), and with a seawater Mg content of 1.29 g/L (Stumm and Morgan, 1981). CO₂ concentration was obtained by difference between 100 and the sum of all element oxide weight percent, then converted in element weight percent.

	Calcite (wt%)	Dolomite (wt%)	X_n (mass change in gram)	X_n (mass change in %)	Fluid composition in equilibrium with 3.32L of brine source (mg/L)	Fluid composition in equilibrium with 7.84L seawater source (mg/L)	K_D^{Elem-} Ca
Al	-	-	-	-	-	-	-
Fe	0.27	1.08	0.694	255	-	-	-
Mn	0.01	0.02	0.002	15	-	-	-
Mg	0.42	11.75	10.117	2384	-	-	-
Ca	39.28	21.50	-19.989	-51	6026	2549	-
Na	-	-	-	-	-	-	-
K	-	-	-	-	-	-	-
C	11.99	13.37	-0.004	0	1.082	0.457	-
Li	-	-	-	-	-	-	-
B	-	-	-	-	-	-	-
Sc	-	-	-	-	-	-	-
51V	5.34E-04	4.02E-04	-1.74E-04	-33	5.24E-02	2.21E-02	2.15
Cr	-	-	-	-	-	-	-
Ni	-	-	-	-	-	-	-
As	-	-	-	-	-	-	-
Ba	-	-	-	-	-	-	-
Zn	6.95E-04	2.46E-03	1.51E-03	218	-	-	-

Rb	2.30E-04	1.03E-04	-1.38E-04	-60	4.15E-02	1.75E-02	0.70
Sr	3.24E-02	2.56E-03	-3.01E-02	-93	9.076	3.839	0.08
Y	4.18E-04	3.19E-04	-1.31E-04	-31	3.96E-02	1.68E-02	2.26
La	3.73E-04	1.79E-04	-2.13E-04	-57	6.42E-02	2.71E-02	0.78
Ce	5.61E-04	1.91E-04	-3.90E-04	-70	1.18E-01	4.98E-02	0.45
Pr	8.26E-05	3.34E-05	-5.26E-05	-64	1.59E-02	6.71E-03	0.59
Nd	3.41E-04	1.36E-04	-2.19E-04	-64	6.62E-02	2.80E-02	0.58
Sm	7.10E-05	2.80E-05	-4.59E-05	-65	1.38E-02	5.85E-03	0.57
Eu	1.64E-05	6.30E-06	-1.07E-05	-66	3.24E-03	1.37E-03	0.54
Gd	7.17E-05	3.90E-05	-3.67E-05	-51	1.11E-02	4.68E-03	0.99
Tb	1.03E-05	5.00E-06	-5.82E-06	-56	1.75E-03	7.42E-04	0.80
Dy	6.03E-05	3.45E-05	-2.94E-05	-49	8.85E-03	3.74E-03	1.09
Ho	1.25E-05	7.00E-06	-6.22E-06	-50	1.88E-03	7.93E-04	1.05
Er	3.07E-05	2.09E-05	-1.20E-05	-39	3.60E-03	1.52E-03	1.63
Tm	4.40E-06	1.90E-06	-2.70E-06	-61	8.13E-04	3.44E-04	0.66
Yb	2.17E-05	1.68E-05	-6.63E-06	-31	2.00E-03	8.46E-04	2.35
Lu	3.00E-06	1.30E-06	-1.83E-06	-61	5.53E-04	2.34E-04	0.66
Pb	1.05E-03	1.57E-04	-9.14E-04	-87	2.75E-01	1.17E-01	0.16
Th	-	-	-	-	-	-	-
U	1.38E-04	5.30E-05	-9.02E-05	-65	2.72E-02	1.15E-02	0.55

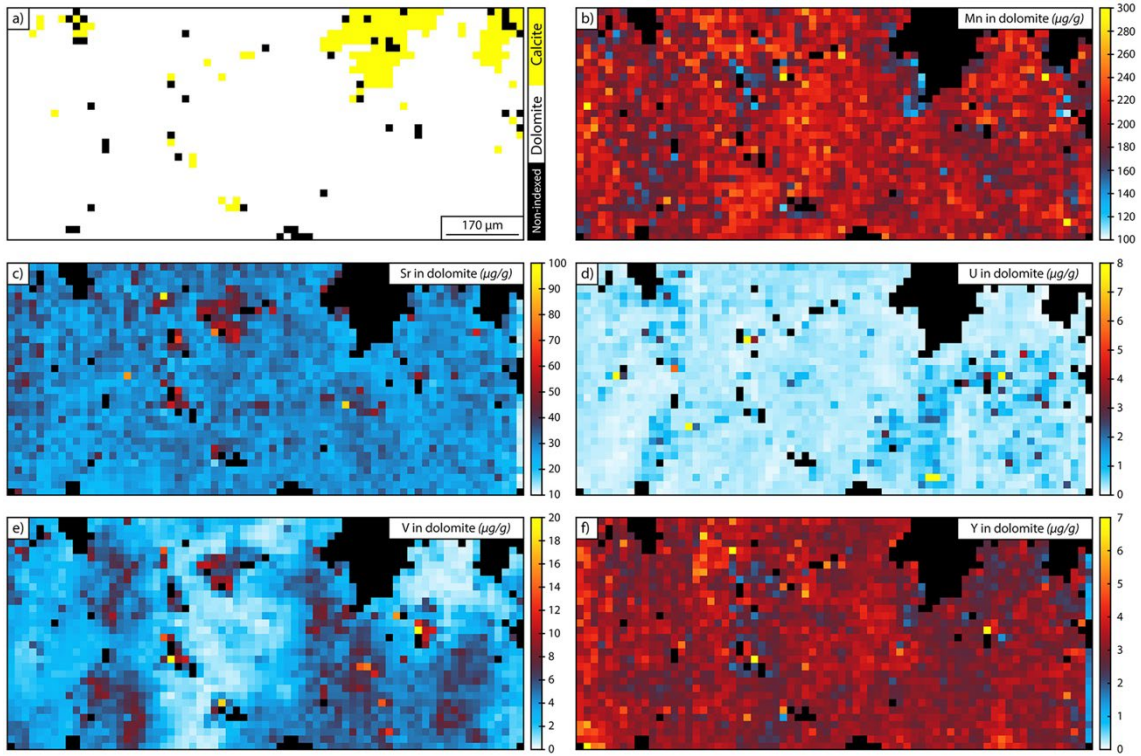


Fig. 4. LA-ICP-MS maps of dolostone sample (BEN 10) with respective phase map (a) and Mn (b), Sr (c), U (d), V (e), Y (f) composition in dolomite. 36 maps were generated but for sake of clarity and simplicity, only 5 are presented with Mn, U and V, redox sensitive elements. Petrographic image is presented in Fig. 3c.

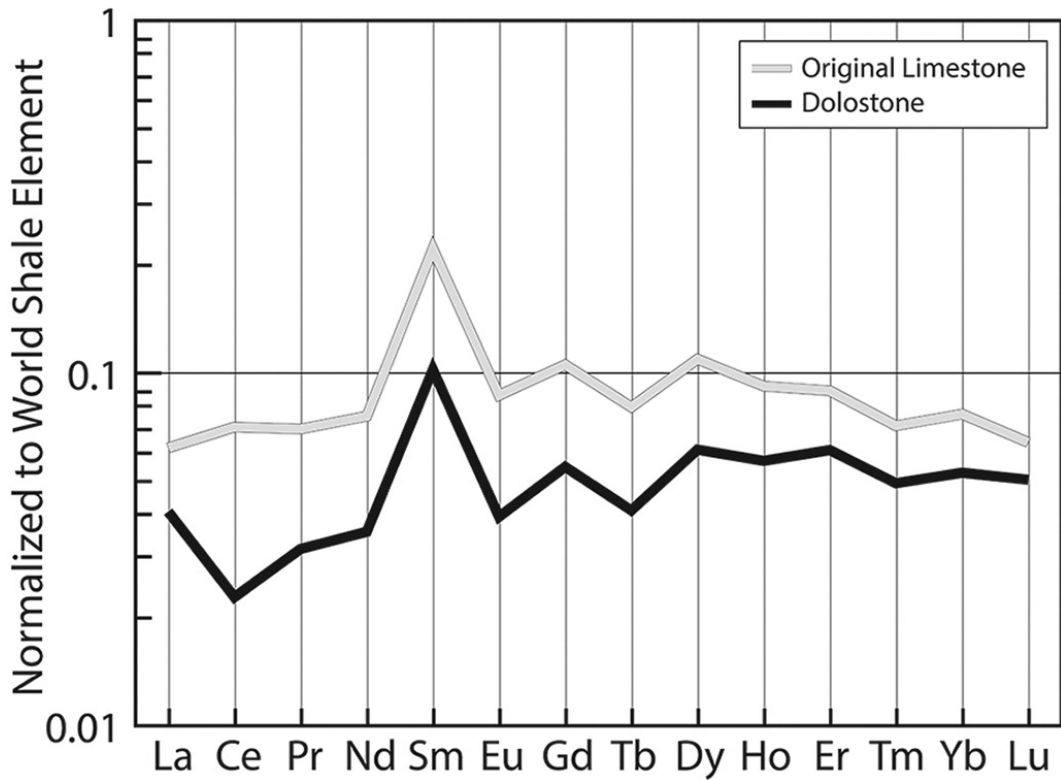


Fig. 5. Spider diagram for limestone and dolostone of the Benassal Formation normalized to world shale (Piper, 1974).

4.3. Mass balance calculations

Results of mass balance calculations are listed below for the dolomitization reaction of the Meillon Formation, the Pine Point Formation and the Benassal Formation. Based on Centrella et al. (2020), calcite density was estimated at 2.71 g.cm^{-3} and dolomite density at 2.84 g.cm^{-3} for the Meillon Formation. Dolomitization was associated with a volume change of $-11.3 \text{ vol}\%$ (Fig. 6). The authors also showed that dolomitization was accompanied by an important element redistribution between the initial calcite and the resulting dolomite, with gains of Li, B, Na, Mg, Sc, Ti, V, Cr, Zn, Mn, Th and U, and loss of Ca, Al, K, Mn, Ni, As, Rb, Sr, Pb, Y and REE, compared to the original limestone composition (Table 1, Fig. 7a). Overall, mass balance calculations demonstrate that 100 g of calcite only made $\sim 93 \text{ g}$ of dolomite (Eq. 6):

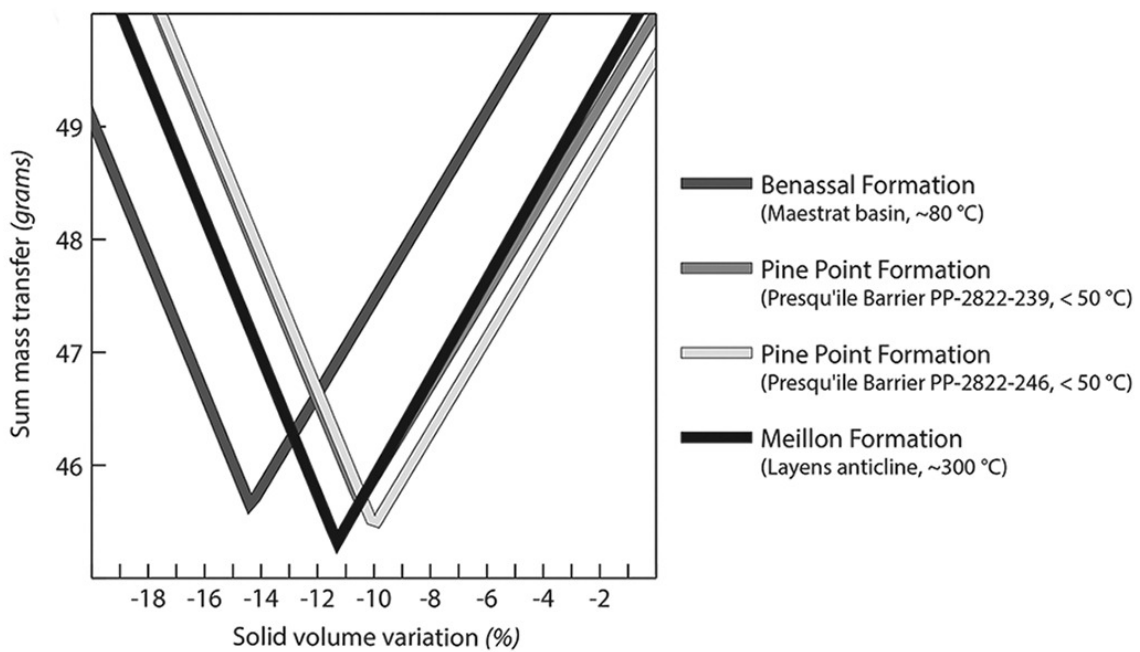
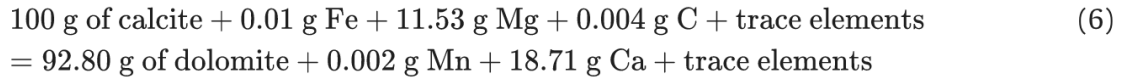


Fig. 6. Sum of gains and losses of elements as a function of the volume change during the reaction for the dolomitization of the Meillon, Pine Point and Benassal formations.

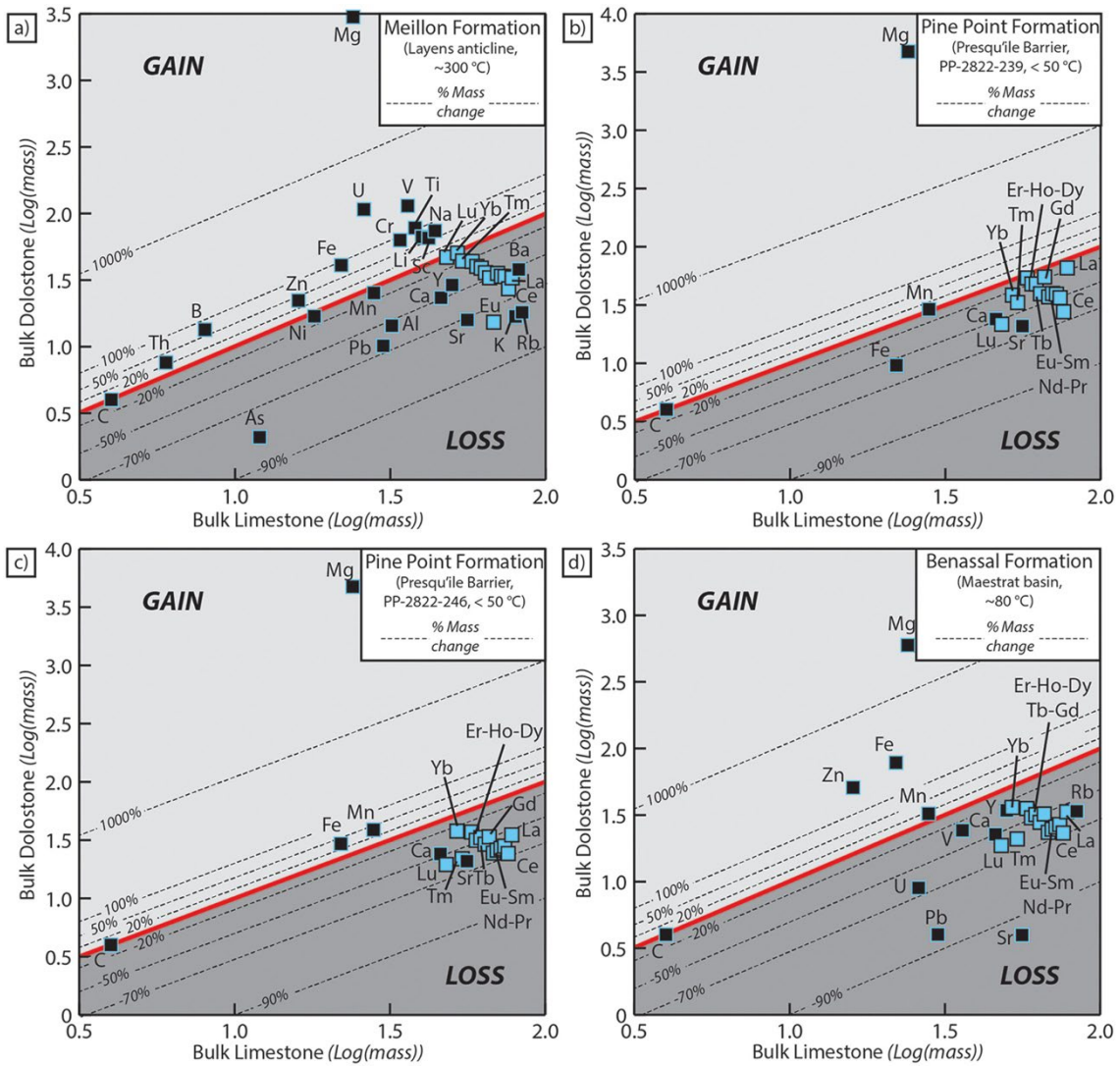
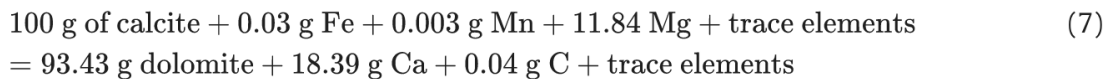


Fig. 7. Isocon diagrams (Grant, 1986, Grant, 2005) for the three localities using the data obtained from the Gresens analysis.

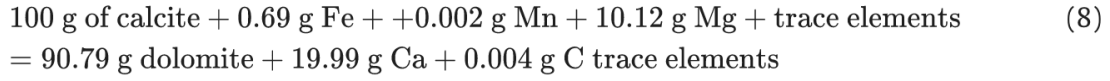
This reaction corresponds to a net mass loss of $\sim 7\%$, using the estimated decrease in volume of 11.3 vol%. Assuming a cubic meter of original limestone, this represents ~ 190 kg of material to be progressively transported out via the fluid phase as the reaction proceeds, supporting the establishment of a long-lasting fluid flux (Ague, 1991, Ague, 1994; Ferry, 1994; Yardley et al., 2014; Centrella et al., 2015, Centrella et al., 2016; Ague, 2017; Centrella et al., 2018; Centrella, 2019).

For the Pine Point Formation, using the bulk rock composition of the limestone and dolostone samples with their respective densities of 2.71 and $2.84 \text{ g}\cdot\text{cm}^{-3}$, the volume change estimated by minimizing the flux of mass transfer is about -10.5 vol% (Fig. 5). Overall, 100 g of calcite only made ~ 94 g of dolomite (net mass loss of $\sim 6\%$), as shown by Eq. 7 for sample PP-2822-246 (more details in Table 2 and Fig. 7b and c):



Considering sample PP-2822-239 instead of PP-2822-246 as the precursor limestone gives similar results except a slight change of the amount of Fe lost during dolomitization (Fig. 7b). For the Benassal Formation, the average chemical composition of calcite and dolomite are presented in Table 3. Densities of calcite and dolomite were estimated at 2.71 and $2.85 \text{ g}\cdot\text{cm}^{-3}$,

respectively, while volume change was estimated at about -14.4 vol% from the mass balance calculations (Fig. 5). Overall, 100 g of calcite only made ~ 91 g of dolomite, corresponding to a net mass loss of $\sim 9\%$ (Eq. 8, Table 3, and Fig. 7d):



4.4. Estimation of the amount and composition of fluid necessary to dolomitization

As described in the method section, the estimation of the amount of aqueous solution needed to dolomitize the initial limestone requires to know the actual mass transfer of elements during the reaction. For the case of the Meillon Formation, according to the mass balance model, 11.53 g of Mg is required to replace 100 g calcite by dolomite (92.8 g) (Eq. 5). Considering an initial fluid with a seawater Mg content (1.29 g/L), this corresponds to 8.94 L /100 g of calcite, which is equivalent to ~ 242 m³ of fluid required for the dolomitization of 1 m³ of limestone. Considering instead an initial fluid with a brine Mg content (3.05 g/L), 3.78 L are required to dolomitize 100 g of calcite, equivalent to ~ 102 m³ of fluid for 1 m³ of limestone. For the both initial Mg concentrations in the initial fluid, the minimum concentrations present in the fluids after dolomitization as calculated from the mass balance equations are presented in Table 1 and plotted in Fig. 8a and c.

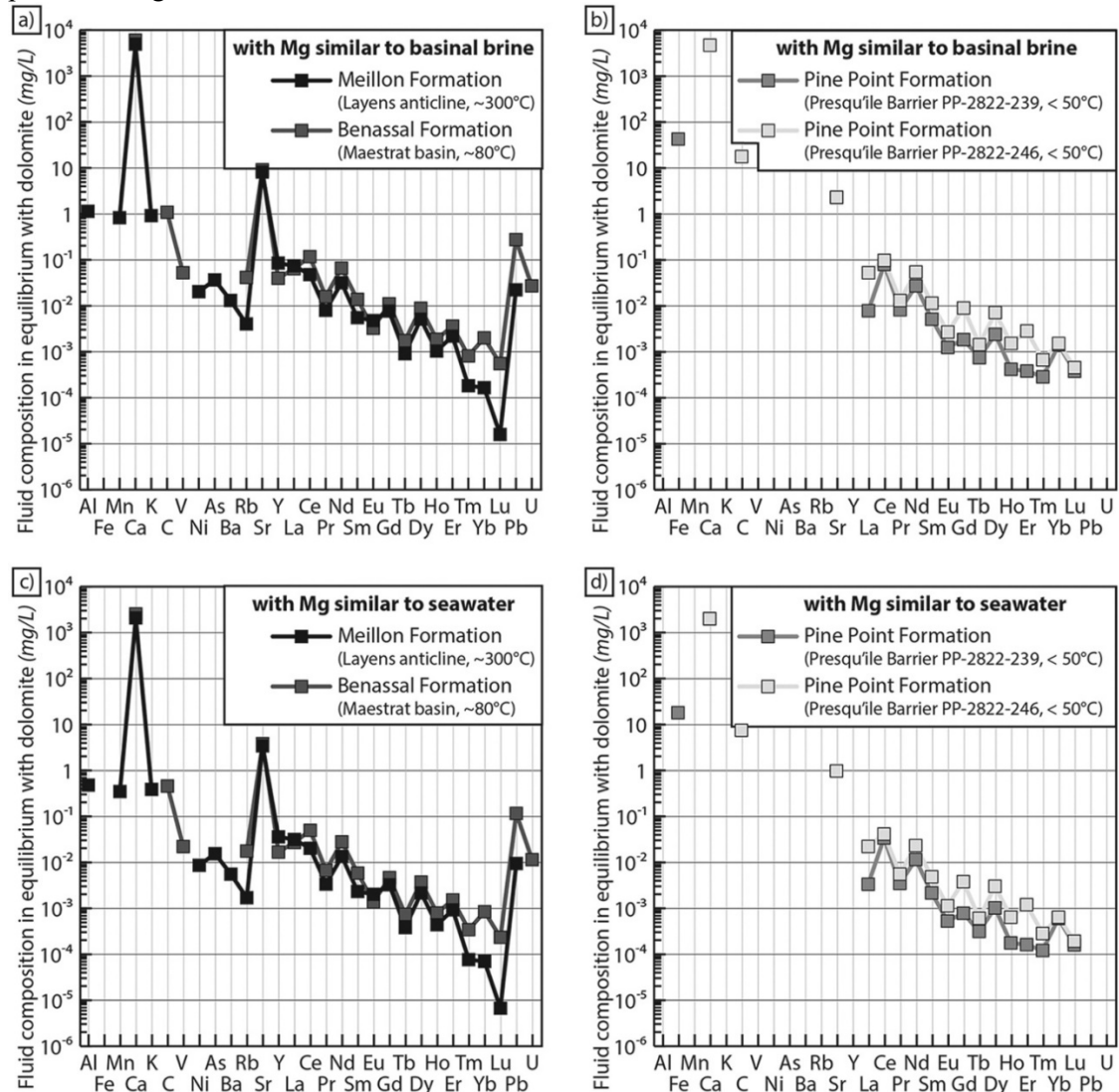


Fig. 8. Element concentrations in water after dolomitization, as calculated for initial waters with Mg concentrations similar to basinal brine (a and b) and to seawater (c and d). To gain in visibility, Pine Point data have been separated from the two others.

For the Pine Point Formation, 11.84 g of Mg is needed to produce 93.43 g of dolomite out of 100 g of calcite (Eq. 6). If the dolomitizing water has a seawater Mg content, 9.18 L are required for 100 g of calcite, equivalent to $\sim 249 \text{ m}^3$ of seawater per m^3 of original limestone. If the original fluid has a Mg content of a basinal brine, the volume decreases to 3.88 L/100 g of calcite, or $\sim 105 \text{ m}^3$ of fluid by m^3 of original limestone. For the both initial Mg concentrations in the initial fluid, the minimum concentrations present in the fluids after dolomitization are presented in Fig. 8b and c.

Finally, for the Benassal Formation, 10.12 g of Mg is required to dolomitize 100 g of calcite, which results in 90.79 g of dolomite (Eq. 7). Using a fluid with a Mg concentration identical to that of seawater, the volume needed for dolomitization is 7.84 L/100 g of calcite, equivalent to $\sim 213 \text{ m}^3$ per m^3 of original limestone. Considering a basinal brine, the volume decreases to 3.32 L/100 g of calcite, or $\sim 90 \text{ m}^3$ by m^3 of original limestone. The minimum concentrations present in the two types of fluids after dolomitization are presented in Fig. 8b and c.

4.5. Exchange partition coefficients

For the Layens samples, the exchange partition coefficients calculated with Eq. 3 range from 0.20 (As) to 47.22 (Lu) (Table 1). For elements other than the REE, the $K_D^{\text{REE}-\text{Ca}}$ values are mostly lower than one, except for Ni, Mn, and Y. For the rare earth elements, the $K_D^{\text{REE}-\text{Ca}}$ values strongly increase between the light REE (LREE), where they are lower than one, and the heavy REE (HREE), where they reach the highest values. This is more important for the lighter than for the heavier REEs (Fig. 9).

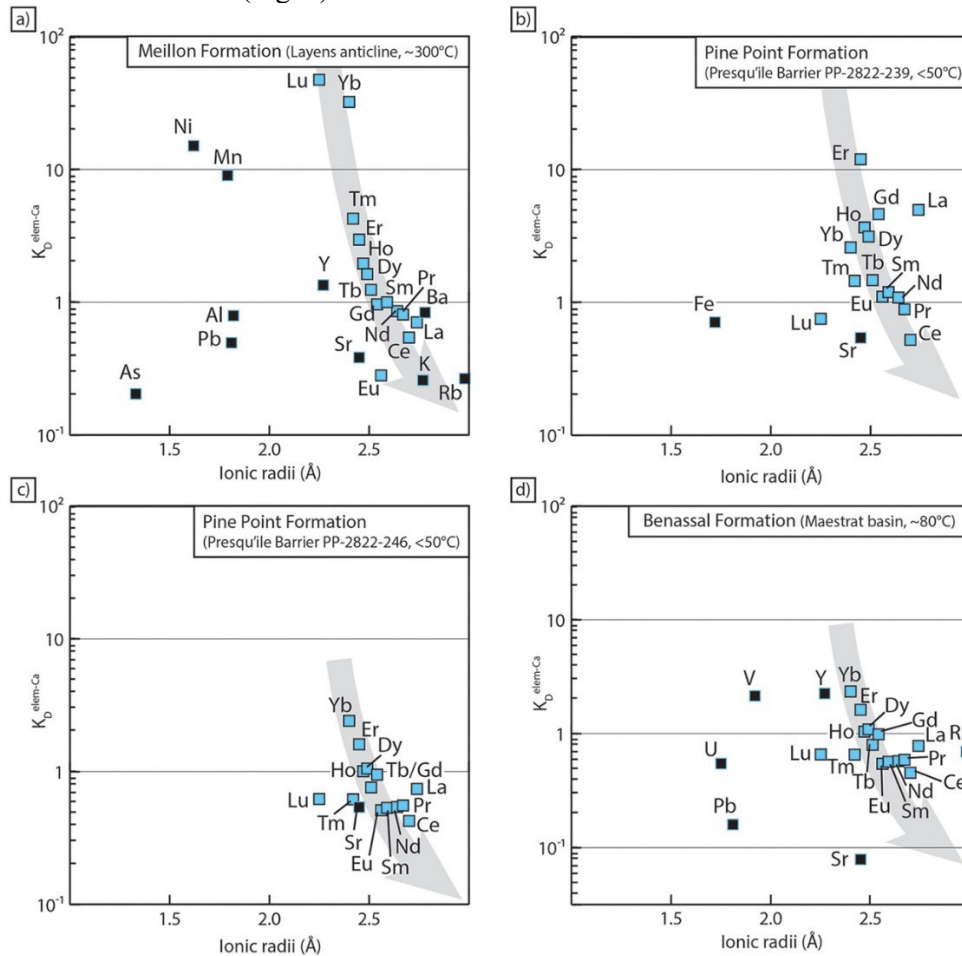


Fig. 9. Diagram summing data obtained for $K_D^{\text{Element}-\text{Ca}}$ for the Meillon (a), Benassal (b) and Pine Point (c and d) formations with the associated relationship as a function of element ionic radius. Original data are presented in Table 1, Table 2, Table 3.

For the Pine Point Formation, the exchange partition coefficients slightly differ between the two original limestone samples. For sample PP-2822-239, the $K_D^{\text{REE-Ca}}$ values range from 0.52 (Ce) to 11.92 (Er). Elements other than the REE (Fe and Sr) show values lower than one (0.71 and 0.54, respectively), whereas most REE present coefficients above unity, without clear trend between the LREE and the HREE (for sample PP-2822-246, they range from 0.43 (Ce) to 2.41 (Yb) (Table 2). The $K_D^{\text{Sr-Ca}}$ value (0.74) is close to the other sample, but most REE have values lower than 1 or close to unity with a slightly increasing trend except for the 3 heaviest REE (Fig. 9).

Regarding the Benassal Formation, the exchange partition coefficients range from 0.08 (Sr) to 2.35 (Yb) (Table 3). The rare earth elements present very low $K_D^{\text{REE-Ca}}$ values, from ~ 0.61 (LREE) to ~ 1.48 (HREE). As for the Meillon and Pine Point formations, they globally increase between the LREE and the HREE, with a few exceptions (Table 3). Considering the REEs for all samples, there is overall a positive correlation between the $K_D^{\text{REE-Ca}}$ and the element mass (Fig. 9). The trend of $K_D^{\text{REE-Ca}}$ from heavy to lightest for the Pine Point and for the Benassal Formation range from 12 to 0.52 and from 2 to 0.45 respectively. Both are less spread than the trend from the Meillon Formation ranging from 47 to 0.28.

5. Discussion

5.1. Interest of the mass balance approach for the study of metasomatic reactions

The approach presented here allows the calculation of mass transfers associated with metasomatic reactions such as dolomitization. Simple in its implementation, since it only requires the study of the solid phases before and after the reaction, it nevertheless combines advanced analytical techniques such as the analysis of the elemental concentration of minerals by LA-ICP-MS, and the use of equations widely proven since the pioneering work of Gresens (1967). We have shown that simple mass balances can provide fundamental information on the chemical balances associated with metasomatism. It is important to remind that calculations assume that only one fluid controls the reaction, and that its chemical composition remains constant during the reaction. In other words, this method can only calculate the composition of last fluid that reacted with the calcite during dolomitization, so it is not suited to assess complex diagenetic history. Furthermore, the average major and trace element chemical composition for dolomite obtained with EPMA and LA-ICP-MS without any information about the crystallography (cathodoluminescence and X-Ray diffraction) implies that studied dolomites can be recrystallized. Their chemical composition can represent their resetting events more than their original dolomitization event. In addition to being able to calculate the amount of material that must be supplied by the fluid phase to allow the reaction to take place, and/or that must be subtracted at the end of the reaction, it is possible to (i) calculate the volumes of fluids required for the reaction, (ii) propose a theoretical composition of a fluid whose composition would be solely dictated by the reaction, and finally (iii) derive minimum values for exchange partition coefficients associated with the reaction. As discussed below, the calculation of the volume of fluid required for the reaction is carried out on the basis of an element chosen as being fixed (Mg for dolomite). In our case, the choice of Mg concentrations comparable to seawater or brine is based on the assumed origin of most dolomitizing fluids in nature. In the case studies presented here, seawater is implied for the Pine Point Formation (Qing and Mountjoy, 1994c; Qing, 1998; Adams et al., 2000), and brines for the Meillon and the Benassal Formations ((Martín-Martín et al., 2010; Martín-Martín et al., 2013; Martín-Martín et al., 2015); Motte, 2020). However, in general, volume estimates, although inherently uncertain due to the absence of the fluid at the origin of metasomatism, can provide additional constraints on the conditions of the mineralogical transformation considered. Similarly, calculations of the theoretical composition of the fluid after the reaction give minimum concentration values, i.e. the fluid that enabled the metasomatic reaction necessarily had values greater than or equal to those proposed, again on the basis of an element of fixed initial composition. Finally, the calculations of

exchange partition coefficients also correspond to minimum values. However, in this last case, several observations suggest that in the case of dolomitization the calculated K_D make sense, and are compatible with a reaction at equilibrium. First, of the trace elements other than REE that can be compared between the Meillon and Benassal formations (Rb, Sr, Y), the K_D values are quite similar, with K_D^{Rb-Ca} and K_D^{Y-Ca} of 0.27–0.70 and 1.37–2.27, respectively, and K_D^{Sr-Ca} values of 0.38 for Meillon and 0.08 for Benassal. These values are also close to the ones obtained by Baker and Burns (1985) from the analysis of dolomites and associated pore waters (~ 0.06), and to the ones obtained experimentally by Jacobson and Usdowski (1976) (0.048). Second, the decrease in ionic radii from the LREEs to the HREEs is expected to favor the incorporation of the heaviest REEs in the dolomite crystal lattice during precipitation (White, 2013). Such a correlation between the ionic radius of the REEs and the K_D is generally observed (Fig. 8, Fig. 9). Moreover, with the exception of Yb and Lu from the Meillon Formation, the K_D^{REE-Ca} do not change significantly between the studied sites. In a more general way, the increase in K_D^{REE-Ca} values from the LREEs to the HREEs is logically accompanied by a decrease in their concentration in the fluid phase (Fig. 8), in agreement with the known geochemical behavior of REEs (White, 2013). The fact that K_D^{REE-Ca} from Pine Point and the Benassal Formation is less spread than the Meillon Formation can be due to a different fluid source or kinetic effect. To our knowledge, there is no other element of which K_D were successfully obtained experimentally for dolomite, so we cannot discuss further the validity of the K_D of other elements like Fe, Mn or Na.

5.2. Insights on the dolomitization process

The three studied examples describe dolomitization reactions occurring at different P – T conditions (~ 50 to ~ 300 °C), from different fluid sources (seawater, basinal brine, and water having likely interacted with evaporites), and in different geodynamic contexts. Despite these differences, similar patterns of solid volume changes (Fig. 6), major and trace element concentrations in the fluid phase after dolomitization (Fig. 8) and K_D variations (Fig. 9). First, in the three case studies, mass loss through the fluid phase is very close, ranging from -9 to -6% . As suggested by Centrella et al. (2020) for the Meillon Formation in the Layens anticline, and confirmed with the examples of the Pine Point and the Benassal formations, dolomitization appears to be a loss-of-mass reaction regardless of the T conditions and the fluid sources. These findings strongly suggest similar mechanisms of calcite-to-dolomite replacement at the sample scale, irrespective of the geologic context. Using the result of the mass balance equation, it is also possible to estimate the amount of fluid required to replace a fixed quantity of original calcite considering a fixed Mg concentration in the input fluid. For all three chosen examples, using an Mg concentration similar to seawater, around ~ 230 m³ of aqueous fluid is required to replace 1 m³ of limestone. This reduces to ~ 100 m³ with if a brine source is considered. These high volumes can be compared to the magnitude of fluid fluxes through rocks undergoing metasomatism, which are still under debate but generally point to important values (Ague, 1994; Ferry, 1994; Centrella et al., 2015; Centrella et al., 2016). Regarding dolomitization, previous work on the Benassal Formation estimated that the total volume of dolomitized rock in the Benicàssim area of 60 km² was on the order of $4 \cdot 10^9$ m³ (Gomez-Rivas et al., 2014). Using a thermodynamic approach, these same authors estimated a minimum of $5 \cdot 10^{11}$ m³ of aqueous fluid in order to dolomitize the original limestone. Using our method, we obtain identical values ranging from $\sim 9 \cdot 10^{11}$ m³ for seawater as a source, and $\sim 4 \cdot 10^{11}$ m³ for brine. Other estimates of the volume of water implied in massive dolomitization have been proposed in Gregg (1985) in the Bonnetterre Dolomite, Southeastern Missouri. They reach $3.5 \cdot 10^{11}$ m³ of basinal brine for a total volume of dolostone of $1.1 \cdot 10^9$ m³, which corresponds to 350 m³/m³ of limestone. In Cooper and Tindall (1994), they reach 230 m³ of seawater per m³ of limestone for the Tertiary limestones of central Florida. Overall, these volumes are of the same order of magnitude as the ones deduced from the mass balance approach. These results, once again, support the idea that the dolomitization process is achieved through comparable mechanisms whatever the geologic context considered. With the growing development of fast concentration analyses such as the

LA-ICP-MS technique, additional dolomitization fronts could be easily studied with the mass balance approach, thereby providing additional results in support of the ones presented here.

6. Conclusions

The proposed method combines in situ analysis to a mass balance model. Applied to various natural case of dolomitization, it allowed to (i) calculate the minimal amount of water necessary for complete calcite-dolomite replacement, (ii) calculate the composition of a fluid whose dissolved content would be provided by the reaction, and (iii) the exchange partition coefficient for most element involved in the reaction. For the three selected sites (Meillon Formation in the Layens anticline, Pine Point Formation in the Presqu'île Barrier, and Benassal Formation in the Maestrat Basin), which are characterized by different conditions of dolomitization and geodynamic environments, the reaction is clearly associated with a loss of mass through the fluid phase. Mass balance calculations suggest that significant amounts of water are required for dolomitization, reaching $\sim 240 \text{ m}^3 / 1 \text{ m}^3$ of limestone considering seawater as the initial fluid. In addition, consistent exchange partition coefficients are obtained, with $K_D^{\text{Sr-Ca}}$ in agreement with experimental data for different temperature and fluid compositions. As a general concept of fluid mediated mineral replacement, the proposed approach is applicable not only to dolomitization, but to other mineralogical replacement reactions such as olivine serpentinization, for which much more experimental data on trace element behavior are already available. This specific reaction has effects on petrophysical and geochemical processes in the lithosphere because it induces fracturing and generates fluid pathways to hydrate original impermeable rocks. The mechanism linking fracture propagation (i.e. a positive solid volume variation) to reaction and associated mass transfer, is still not fully understood.

Declaration of Competing Interest

The authors declare that they have no known competing financial interests or personal relationships that could have appeared to influence the work reported in this paper.
Stephen Centrella.

Acknowledgement

This work is funded by the project TXM-R2 (Institut Carnot ISiFOR), S.C. and N.E.B. are funded through the isite-E2S, supported by the ANR PIA and the Région Nouvelle-Aquitaine.

Data availability

No data was used for the research described in the article.

References

- Adams, J.J., Rostron, B.J., Mendoza, C.A., 2000. Evidence for two-fluid mixing at Pine Point, NWT. *J. Geochem. Explor.* 69-70, 103–108.
- Ague, J.J., 1991. Evidence for major mass transfer and volume strain during regional metamorphism of pelites. *Geology* 19, 855–858.
- Ague, J.J., 1994. Mass transfer during Barrovian metamorphism of pelites, South-Central Connecticut. I: evidence for changes in composition and volume. *Am. J. Sci.* 294, 989–1057.
- Ague, J.J., 2017. Element mobility during regional metamorphism in crustal and subduction zone environments with a focus on the rare earth elements (REE). *Am. Mineral.* 102, 1796–1821.
- Ague, J.J., Nicolescu, S., 2014. Carbon dioxide released from subduction zones by fluid-mediated reactions. *Nat. Geosci.* 7, 355–360.

- Al-Helal, A.B., Whitaker, F.F., Xiao, Y., 2012. Reactive transport modeling of brine reflux: dolomitization, anhydrite precipitation, and porosity evolution. *J. Sediment. Res.* 82, 196–215.
- Baker, P.A., Burns, S.J., 1985. Occurrence and formation of dolomite in organic-rich continental margin sediments. *Bulletin* 69.
- Banner, J.L., Hanson, G.N., 1990. Calculation of simultaneous isotopic and trace element variations during water-rock interaction with applications to carbonate diagenesis. *Geochim. Cosmochim. Acta* 54, 3123–3137.
- Barale, L., Bertok, C., Salih Talabani, N., d’Atri, A., Martire, L., Piana, F., Pr at, A., 2016. Very hot, very shallow hydrothermal dolomitization: an example from the Maritime Alps (north-West Italy-south-east France). *Sedimentology* 63, 2037.2065.
- Baumgartner, L., Ferry, J.M., 1991. A model for coupled fluid-flow and mixed-volatile mineral reactions with applications to regional metamorphism. *Contrib. Mineral. Petrol.* 106, 273.285.
- B n ezeth, P., Berninger, U.-N., Bovet, N., Schott, J., Oelkers, E.H., 2018. Experimental determination of the solubility product of dolomite at 50.253. *C. Geochim. Cosmochim. Acta* 224, 262.275.
- Bover-Arnal, T., Martin-Martin, J.D., Gomez-Rivas, E., Trav e, A., Salas, R., Moreno-Bedmar, J.A., Tom as, S., 2009. Insights into the Upper Aptian Carbonate Succession the South-Eastern Maestrat Basin (E Iberia), pp. 123.128.
- Centrella, S., 2019. The Granulite- to Eclogite- and Amphibolite-Facies Transition: a Volume and Mass Transfer Study in the Lindas Nappe, Bergen Arcs, West Norway, pp. 241.263.
- Centrella, S., Austrheim, H., Putnis, A., 2015. Coupled mass transfer through a fluid phase and volume preservation during the hydration of granulite: an example from the Bergen Arcs, Norway. *Lithos* 236-237, 245.255.
- Centrella, S., Austrheim, H., Putnis, A., 2016. Mass transfer and trace element redistribution during hydration of granulites in the Bergen Arcs, Norway. *Lithos* 262, 1.10.
- Centrella, S., Putnis, A., Lanari, P., Austrheim, H., 2018. Textural and chemical evolution of pyroxene during hydration and deformation: a consequence of retrograde metamorphism. *Lithos* 296-299, 245.264.
- Centrella, S., Beaudoin, N.E., Derluyn, H., Motte, G., Hoareau, G., Lanari, P., Piccoli, F., Pecheyran, C., Callot, J.-P., 2020. Micro-scale chemical and physical patterns in an interface of hydrothermal dolomitization reveals the governing transport mechanisms in nature: case of the Layens anticline, Pyrenees, France. *Sedimentology*.
<https://doi.org/10.1111/sed.12808>.
- Cooper, C.R., Tindall, J.A., 1994. Model for dolomite formation in Northwest Florida. *J. Hydrol.* 157, 367.391.
- Corbella, M., Gomez-Rivas, E., Martin-Martin, J.D., Stafford, S.L., Teixell, A., Griera, A., Trave, A., Cardellach, E., Salas, R., 2014. Insights to controls on dolomitization by means of reactive transport models applied to the Benic assim case study (Maestrat Basin, eastern Spain). *Pet. Geosci.* 20, 41.54.
- Davies, G.R., Smith, L.B., 2006. Structurally controlled hydrothermal dolomite reservoir facies: an overview. *Bulletin* 90, 1641.1690.
- Diehl, S.F., Hofstra, A.H., Koenig, A.E., Emsbo, P., Christiansen, W., Johnson, C., 2010. Hydrothermal zebra dolomite in the Great Basin, Nevada - Attributes and relation to Paleozoic stratigraphy, tectonics, and ore deposits. *Geosphere* 6, 665.690.
- Ferry, J.M., 1994. Overview of the petrologic record of fluid flow during regional metamorphism in northern New Zealand. *Am. J. Sci.* 294, 905.988.
- Gabellone, T., Whitaker, F., 2016. Secular variations in seawater chemistry controlling dolomitisation in shallow reflux systems: insights from reactive transport modelling. *Sedimentology* 63, 1233.1259.
- Garcia, R., Moreno-Bedmar, J.A., Bover-Arnal, T., Company, M., Salas, R., Latil, J.-L., Mart ın-Mart ın, J.D., Gomez-Rivas, E., Bulot, L.G., Delanoy, G., Mart ınez, R., Grauges, A., 2014. Lower cretaceous (Hauterivian-Albian) ammonite biostratigraphy in the Maestrat Basin (E Spain). *J. Iber. Geol.* 40.

- Gasparrini, M., Bechstädt, T., Boni, M., 2006. Massive hydrothermal dolomites in the southwestern Cantabrian Zone (Spain) and their relation to the Late Variscan evolution. *Mar. Pet. Geol.* 23, 543–568.
- Gomez-Rivas, E., Warber, K., Kulzer, F., Bons, P.D., Koehn, D., Martín-Martín, J.D., 2012. Structural evolution of the Benicàssim area (Maestrat basin, NE Spain): insights from fracture and vein analysis. *Geogaceta* 51, 79–82.
- Gomez-Rivas, E., Corbella, M., Martín-Martín, J.D., Stafford, S.L., Teixell, A., Bons, P.D., Griera, A., Cardellach, E., 2014. Reactivity of dolomitizing fluids and Mg source evaluation of fault-controlled dolomitization at the Benicàssim outcrop analogue (Maestrat basin, E Spain). *Mar. Pet. Geol.* 55, 26–42.
- Graf, D.L., 1961. Crystallographic tables for the rhombohedral carbonates. *Am. Mineral.* 46, 1283–1316.
- Grant, J.A., 1986. The Isocon Diagram—a simple solution to Gresens' Equation for Metasomatic Alteration. *Econ. Geol.* 81, 1976–1982.
- Grant, J.A., 2005. Isocon analysis: a brief review of the method and applications. *Phys. Chem. Earth, Parts A/B/C* 30, 997–1004.
- Gregg, J.M., 1985. Regional epigenetic dolomitization in the Bonneterre Dolomite (Cambrian), southeastern Missouri. *Geol* 13, 503.
- Gresens, R.L., 1967. Composition-volume relationships of metasomatism. *Chem. Geol.* 2, 47–65.
- Guimerà, J., Mas, R., Alonso, Á., 2004. Intraplate deformation in the NW Iberian Chain: Mesozoic extension and Tertiary contractional inversion. *J. Geol. Soc.* 161, 291–303.
- Hermann, J., Zheng, Y.-F., Rubatto, D., 2013. Deep Fluids in Subducted Continental Crust. *Elements* 9, 281–287.
- Incerpi, N., Manatschal, G., Martire, L., Bernasconi, S.M., Gerdes, A., Bertok, C., 2020. Characteristics and timing of hydrothermal fluid circulation in the fossil Pyrenean hyperextended rift system: new constraints from the Chaînons Béarnais (W Pyrenees). *Int J Earth Sci (Geol Rundsch)* 110, 1.
- Izquierdo-Llavall, E., Menant, A., Aubourg, C., Callot, J.-P., Hoareau, G., Lahfid, A., Camps, P., Pere, E., 2020. Pre-orogenic folds and syn-orogenic basement tilts in an inverted hyperextended margin: the northern Pyrenees case study. *Tectonics* 39.
- Jackson, S.A., Beales, F.W., 1967. An aspect of sedimentary basin evolution: the concentration of Mississippi Valley-Type ores during late stages of diagenesis. *Bull. Can. Petrol. Geol.* 15, 383–433.
- Jacobson, R.L., Usdowski, H.E., 1976. Partitioning of strontium between calcite, dolomite and liquids: an experimental study under higher temperature diagenetic conditions, and a model for the prediction of mineral pairs for geothermometry. *Contrib. Mineral. Petrol.* 59, 171–185.
- Jochum, K.P., Weis, U., Stoll, B., Kuzmin, D., Yang, Q., Raczek, I., Jacob, D.E., Stracke, A., Birbaum, K., Frick, D.A., Günther, D., Enzweiler, J., 2011. Determination of Reference Values for NIST SRM 610-617 Glasses following ISO guidelines. *Geostand. Geoanal. Res.* 35, 397–429.
- Jonas, L., Müller, T., Dohmen, R., Baumgartner, L., Putlitz, B., 2015. Transport-controlled hydrothermal replacement of calcite by Mg-carbonates. *Geology* 43, 779–782.
- Jonas, L., Müller, T., Dohmen, R., Immenhauser, A., Putlitz, B., 2017. Hydrothermal replacement of biogenic and abiogenic aragonite by Mg-carbonates – Relation between textural control on effective element fluxes and resulting carbonate phase. *Geochim. Cosmochim. Acta* 196, 289–306.
- Kelka, U., Koehn, D., Beaudoin, N., 2015. Zebra pattern in rocks as a function of grain growth affected by second-phase particles. *Front. Phys.* 3, 201.
- Kelka, U., Veveakis, M., Koehn, D., Beaudoin, N., 2017. Zebra rocks: compaction waves create ore deposits. *Sci. Rep.* 7, 14260.
- Kharaka, Y.K., Thordsen, J.J., 1992. Stable isotope geochemistry and origin of waters in sedimentary basins. *Lect. Notes Earth Sci.* 43, 411–466.

- Kirschner, J.P., Barnes, D.A., 2009. Geological sequestration capacity of the Dundee Limestone, Michigan Basin, United States. *Environ. Geosci.* 16, 127–138.
- Koeshidayatullah, A., Corlett, H., Stacey, J., Swart, P.K., Boyce, A., Hollis, C., 2020. Origin and evolution of fault-controlled hydrothermal dolomitization fronts: a new insight. *Earth Planet. Sci. Lett.* 541, 116291.
- Kretz, R., 1982. A model for the distribution of trace elements between calcite and dolomite. *Geochimica et Cosmochimica Acta* 46, 1979–1981.
- Labaume, P., Teixell, A., 2020. Evolution of salt structures of the Pyrenean rift (Châinons Béarnais, France): From hyper-extension to tectonic inversion. *Tectonophysics* 785.
- Lenoble, J.-L., 1992. Les plates-formes carbonatées ouest pyrénéennes du Dogger à l'Albien. PhD, Toulouse, p. 447.
- Machel, H.G., 2004. Concepts and models of dolomitization: a critical reappraisal. *Geol. Soc. Lond., Spec. Publ.* 235, 7–63.
- Martín-Martín, J.D., Travé, A., Gomez-Rivas, E., Sizun, J., Salas, R., Gómez-Gras, D., Vergés, J., 2010. Fault-associated Dolomites in the Benicàssim Area, Maestrat Basin, E. Spain – Macro- to Micro-scale Fluid Flow in Carbon. In: 72nd EAGE Conference and Exhibition incorporating SPE EUROPEC 2010. 72nd EAGE Conference and Exhibition incorporating SPE EUROPEC 2010, Barcelona, Spain. 14 Jun 2010–17 Jun 2010. European Association of Geoscientists & Engineers.
- Martín-Martín, J.D., Gomez-Rivas, E., Travé, A., Salas, R., Vergés, J., 2012. Dolomías controladas por fracturas en carbonatos aptienses de la zona de Benicàssim (SE Cuenca del Maestrat): distribución y características petrográficas. *Geogaceta* 51, 19–22.
- Martín-Martín, J.D., Gomez-Rivas, E., Bover-Arnal, T., Travé, A., Salas, R., Moreno-Bedmar, J.A., Tomás, S., Corbella, M., Teixell, A., Vergés, J., Stafford, S.L., 2013. The Upper Aptian to lower Albian syn-rift carbonate succession of the southern Maestrat Basin (Spain): Facies architecture and fault-controlled stratabound dolostones. *Cretac. Res.* 41, 217–236.
- Martín-Martín, J.D., Travé, A., Gomez-Rivas, E., Salas, R., Sizun, J.-P., Vergés, J., Corbella, M., Stafford, S.L., Alfonso, P., 2015. Fault-controlled and stratabound dolostones in the late Aptian–earliest Albian Benassal Formation (Maestrat Basin, E Spain): Petrology and geochemistry constrains. *Mar. Pet. Geol.* 65, 83–102.
- Meijer Drees, N.C., 1988. The Middle Devonian Sub-Watt Mountain Unconformity across the Tathlina Uplift; District of Mackenzie and Northern Alberta. CSPG Special Publications, Canada, p. 477.
- Möller, P., de Lucia, M., 2020. The impact of Mg²⁺ ions on equilibration of Mg-Ca carbonates in groundwater and brines. *Geochemistry* 80, 125611.
- Moreno-Bedmar, J.A., Company, M., Bover-Arnal, T., Salas, R., Delanoy, G., Maurrasse, F.-M., Grauges, A., Martinez, R., 2010. Lower Aptian ammonite biostratigraphy in the Maestrat Basin (Eastern Iberian Chain, Eastern Spain). A Tethyan transgressive record enhanced by synrift subsidence. *Geol. Acta* 8, 281–299.
- Motte, G., 2020. Dolomitization Characterization of a Carbonate Platform in the Hyper-Extended and Inverted Salt Margin Context: Example of the West Pyrenean Jurassic Carbonate Platform: Caractérisation de la Dolomitisation d'une Plate-Forme carbonatée en Contexte de Marge salifère Hyper-étendue et inversée : Exemple de la Plate-Forme carbonatée Jurassique Ouest-pyrénéenne.
- Motte, G., Hoareau, G., Callot, J.-P., Révillon, S., Piccoli, F., Calassou, S., Gaucher, E.C., 2021. Rift and salt-related multi-phased dolomitization: example from the northwestern Pyrenees. *Mar. Pet. Geol.* 126.
- Mouthereau, F., Filleaudeau, P.-Y., Vacherat, A., Pik, R., Lacombe, O., Fellin, M.G., Castellort, S., Christophoul, F., Masini, E., 2014. Placing limits to shortening evolution in the Pyrenees: Role of margin architecture and implications for the Iberia/Europe convergence. *Tectonics* 33, 2283–2314.
- Mozafari, M., Swennen, R., Balsamo, F., El Desouky, H., Storti, F., Taberner, C., 2019. Fault-controlled dolomitization in the Montagna Dei Fiori Anticline (Central Apennines, Italy): record of a dominantly pre-orogenic fluid migration. *Solid Earth* 10, 1355–1383.

- Nader, F.H., López-Horgue, M.A., Shah, M.M., Dewit, J., Garcia, D., Swennen, R., Iriarte, E., Muchez, P., Caline, B., 2012. The Ranero Hydrothermal Dolomites (Albian, Karrantza Valley, Northwest Spain): implications on conceptual dolomite models. In: *Oil Gas Sci. Technol. – Rev.*, 67. IFP Energies nouvelles, pp. 9–29.
- Piper, D.Z., 1974. Rare earth elements in the sedimentary cycle: a summary. *Chem. Geol.* 14, 285–304.
- Puigdefàbregas and Souquet, 1986. Tecto-sedimentary cycles and depositional sequences of Mesozoic and Tertiary from the Pyrenees. *Tectonophysics* 129, 173–203.
- Putnis, A., 2002. Mineral replacement reactions: from macroscopic observations to microscopic mechanisms. *Mineral. Mag.* 66, 689–708.
- Putnis, A., 2009. Mineral Replacement Reactions. *Rev. Mineral. Geochem.* 70, 87–124.
- Qing, H., 1998. Petrography and geochemistry of early-stage, fine- and medium-crystalline dolomites in the Middle Devonian Presqu'île Barrier at Pine Point, Canada. *Sedimentology* 45, 433–446.
- Qing, H., Mountjoy, E.W., 1990. Petrography and diagenesis of Middle Devonian Presqu'île barrier: implications on formation of dissolution vugs and breccias at Pine Point and adjacent subsurface, District of Mackenzie. *Geolog. Survey of Canada* 90-1D, 37–45.
- Qing, H., Mountjoy, E.W., 1994a. Formation of coarsely crystalline, hydrothermal dolomite reservoirs in the presqu'île barrier, Western Canada Sedimentary Basin. *Bulletin* 78.
- Qing, H., Mountjoy, E.W., 1994b. Origin of dissolution vugs, caverns, and breccias in the Middle Devonian Presqu'île barrier, host of Pine Point Mississippi valley-type deposits. *Econ. Geol.* 89, 858–876.
- Qing, H., Mountjoy, E.W., 1994c. Rare earth element geochemistry of dolomites in the Middle Devonian Presqu'île barrier, Western Canada Sedimentary Basin: implications for fluid-rock ratios during dolomitization. *Sedimentology* 41, 787–804.
- Reeder, R.J., Dollase, W.A., 1989. Structural variation in the dolomite-ankerite solid solution series; an X-ray, Moessbauer, and TEM study. *Am. Mineral.* 74, 1159–1167.
- Roca, E., Guimerà, J., 1992. The Neogene structure of the eastern Iberian margin: Structural constraints on the crustal evolution of the Valencia trough (western Mediterranean). *Tectonophysics* 203, 203–218.
- Rodríguez-López, J.P., Meléndez, N., Soria, A.R., Liesa, C.L., van Loon, A.J., 2007. Lateral variability of ancient seismites related to differences in sedimentary facies (the synrift Escucha Formation, mid-cretaceous, eastern Spain). *Sediment. Geol.* 201, 461–484.
- Salardon, R., Carpentier, C., Bellahsen, N., Pironon, J., France-Lanord, C., 2017. Interactions between tectonics and fluid circulations in an inverted hyper-extended basin: example of mesozoic carbonate rocks of the western North Pyrenean Zone (Chaînons Béarnais, France). *Mar. Pet. Geol.* 80, 563–586.
- Salas, R., Casas, A., 1993. Mesozoic extensional tectonics, stratigraphy and crustal evolution during the Alpine cycle of the eastern Iberian basin. *Tectonophysics* 228, 33–55.
- Salas, R., Guimeri, J., Mas, R., Martin-Closas, C., Meléndez, A., Alonso, A., 2001. Evolution of the Mesozoic Central Iberian Rift System and its Cainozoic inversion (Iberian chain). *Mém. Mus. Natl. Hist. Nat.* 1993 (186), 145–186.
- Slaughter, M., Hill, R.J., 1991. The influence of organic matter in organogenic dolomitization: Perspective. *J. Sediment. Petrol.* 61, 296–303.
- Staude, S., Bons, P.D., Markl, G., 2009. Hydrothermal vein formation by extension-driven dewatering of the middle crust: an example from SW Germany. *Earth Planet. Sci. Lett.* 286, 387–395.
- Steinfink, H., Sans, F.J., 1959. Refinement of the crystal structure of dolomite. *Am. Mineral.* 44, 679–682.
- Stumm, W., Morgan, J.J., 1981. *Aquatic Chemistry - an Introduction Emphasizing Chemical Equilibria in Natural Waters.* Wiley, New York.
- Swennen, R., Dewit, J., Fierens, E.L., Muchez, P., Shah, M., Nader, F., Hunt, D., 2012. Multiple dolomitization events along the Pozalagua Fault (Pozalagua Quarry, Basque-Cantabrian Basin, Northern Spain). *Sedimentology* 59, 1345–1374.

- Teixell, A., Labaume, P., Lagabriele, Y., 2016. The crustal evolution of the west-Central Pyrenees revisited: Inferences from a new kinematic scenario. *Compt. Rendus Geosci.* 348, 257–267.
- Thibeau, S., Chiquet, P., Prinet, C., Lescanne, M., 2013. Lacq-Rousse CO2 Capture and Storage Demonstration pilot: Lessons Learnt from Reservoir Modelling Studies. *Energy Procedia* 37, 6306–6316.
- Tomás, S., Comas Nebot, M., Salas, R., 2007. La plataforma carbonatada Aptiense superior de Benicàssim-Orpesa (Cuenca del Maestrat, Cadena Ibérica): modelo de depósito. *Geogaceta* 41, 235–238.
- Vacherat, A., Mouthereau, F., Pik, R., Bernet, M., Gautheron, C., Masini, E., Le Pourhiet, L., Tibari, B., Lahfid, A., 2014. Thermal imprint of rift-related processes in orogens as recorded in the Pyrenees. *Earth Planet. Sci. Lett.* 408, 296–306.
- Wallace, M.W., Both, R.A., Ruano, S.M., Fenoll Hach-Ali, P., Lees, T., 1994. Zebra textures from carbonate-hosted sulfide deposits; sheet cavity networks produced by fracture and solution enlargement. *Econ. Geol.* 89, 1183–1191.
- Warren, J., 2000. Dolomite: occurrence, evolution and economically important associations. *Earth-Sci. Rev.* 52, 1–81.
- Weisheit, A., Bons, P.D., Elburg, M.A., 2013. Long-lived crustal-scale fluid flow: the hydrothermal mega-breccia of Hidden Valley, Mt. Painter Inlier, South Australia. *Int J Earth Sci (Geol Rundsch)* 102, 1219–1236.
- Whitaker, F.F., Smart, P.L., Jones, G.D., 2004. Dolomitization: from conceptual to numerical models. *Geol. Soc. Lond., Spec. Publ.* 235, 99–139.
- White, W., 2013. *Geochemistry*, 55 pp.
- Wilson, E.N., Hardie, L.A., Phillips, O.M., 1990. Dolomitization front geometry, fluid flow patterns, and the origin of massive dolomite thetriassic latemar buildup northern Italy. *Am. J. Sci.* 290, 741–796.
- Yang, L., Yu, L., Liu, K., Jia, J., Zhu, G., Liu, Q., 2022. Coupled effects of temperature and solution compositions on metasomatic dolomitization: significance and implication for the formation mechanism of carbonate reservoir. *J. Hydrol.* 604, 127199.
- Yardley, B.W.D., Rhede, D., Heinrich, W., 2014. Rates of Retrograde Metamorphism and their Implications for the Rheology of the Crust: an Experimental Study. *J. Petrol.* 55, 623–641.